nature communications

Article

https://doi.org/10.1038/s41467-026-70282-w

STIM1-Mitofusin2 interactions tether mitochondria and melanosome contacts that promote melanosome maturation

Received: 23 April 2025

Accepted: 19 February 2026

Published online: 06 March 2026

Check for updates

Isshin Shiiba[1,2] ✉, Yuto Ishikawa[1], Hijiri Oshio[1], Naoki Ito[1], Fuya Yamaguchi[1], Shun Nagashima[3], Hideya Ando[4], Keitaro Umezawa[5], Yuri Miura[5], Yuhei Araiso[6], Koki Nakamura[7], Yusuke Hirabayashi[7,8], Ryoko Inatome[1] & Shigeru Yanagi[1] ✉

Mitochondria form contact sites with multiple organelles to coordinate diverse cellular processes. Melanosomes, lysosome-related organelles, undergo stepwise maturation to synthesize and store melanin, but how they interact with mitochondria remains unclear. Here we show that mitochondria–melanosome contacts dynamically increase during melanosome maturation and are mediated by STIM1–MFN2 interactions. Using a NanoBiT-based reporter system, MiMSBiT (Mitochondria–Melanosome contact reporter applying NanoBiT), to monitor reversible mitochondria–melanosome contacts in living cells, we demonstrate that STIM1 localizes to melanosomes and promotes their contact with mitochondrial MFN2. A transient decrease in melanosomal lumen calcium induces STIM1 clustering and enhances its association with MFN2. These contacts locally increase mitochondrial ATP availability, leading to melanosome lumen acidification via proton channel activation. This acidification facilitates PMEL fibrillation, a key step in melanosome maturation. Together, our findings reveal a mechanism by which mitochondria–melanosome contacts regulate melanosome maturation.

Mitochondria are essential organelles in eukaryotic cells, playing critical roles in ATP synthesis and intracellular signal transduction. To fulfill these functions, mitochondria undergo dynamic cycles of fission and fusion and interact with various organelles[1–4]. Among these interactions, mitochondria-endoplasmic reticulum (ER) contact has been extensively studied using electron microscopy[5]. Previous studies have revealed that a variety of tethering factors, including MFN2[6], form functional scaffolds that facilitate the transport of metabolites, such as calcium and lipids[7–9]. Similarly, mitochondria-melanosome contact has been observed, and MFN2 has been proposed as a potential mediator of this interaction, thereby contributing to the regulation of melanosome biogenesis[10]. However, many aspects of MFN2 involvement in the melanosome maturation process, as well as the dynamics and physiological significance of mitochondria-melanosome contact, remain unclear.

[1]Laboratory of Molecular Biochemistry, Department of Life Science, Faculty of Science, Gakushuin University, Toshima, Japan. [2]Graduate School of Pharmaceutical Sciences, Tohoku University, Sendai, Japan. [3]Laboratory of Regenerative Medicine, School of Life Sciences, Tokyo University of Pharmacy and Life Sciences, Hachioji, Japan. [4]Department of Bioscience, Okayama University of Science, Okayama, Japan. [5]Research Team for Mechanism of Aging, Tokyo Metropolitan Institute for Geriatrics and Gerontology, Itabashi-ku, Japan. [6]Department of Clinical Laboratory Science, Division of Health Sciences, Graduate School of Medical Sciences, Kanazawa University, Kanazawa, Japan. [7]Department of Chemistry and Biotechnology, School of Engineering, The University of Tokyo, Tokyo, Japan. [8]Department of Bioengineering, School of Engineering, The University of Tokyo, Tokyo, Japan. ✉e-mail: isshin.shiiba.b6@tohoku.ac.jp; shigeru.yanagi@gakushuin.ac.jp

https://doi.org/10.1038/s41467-026-70282-w

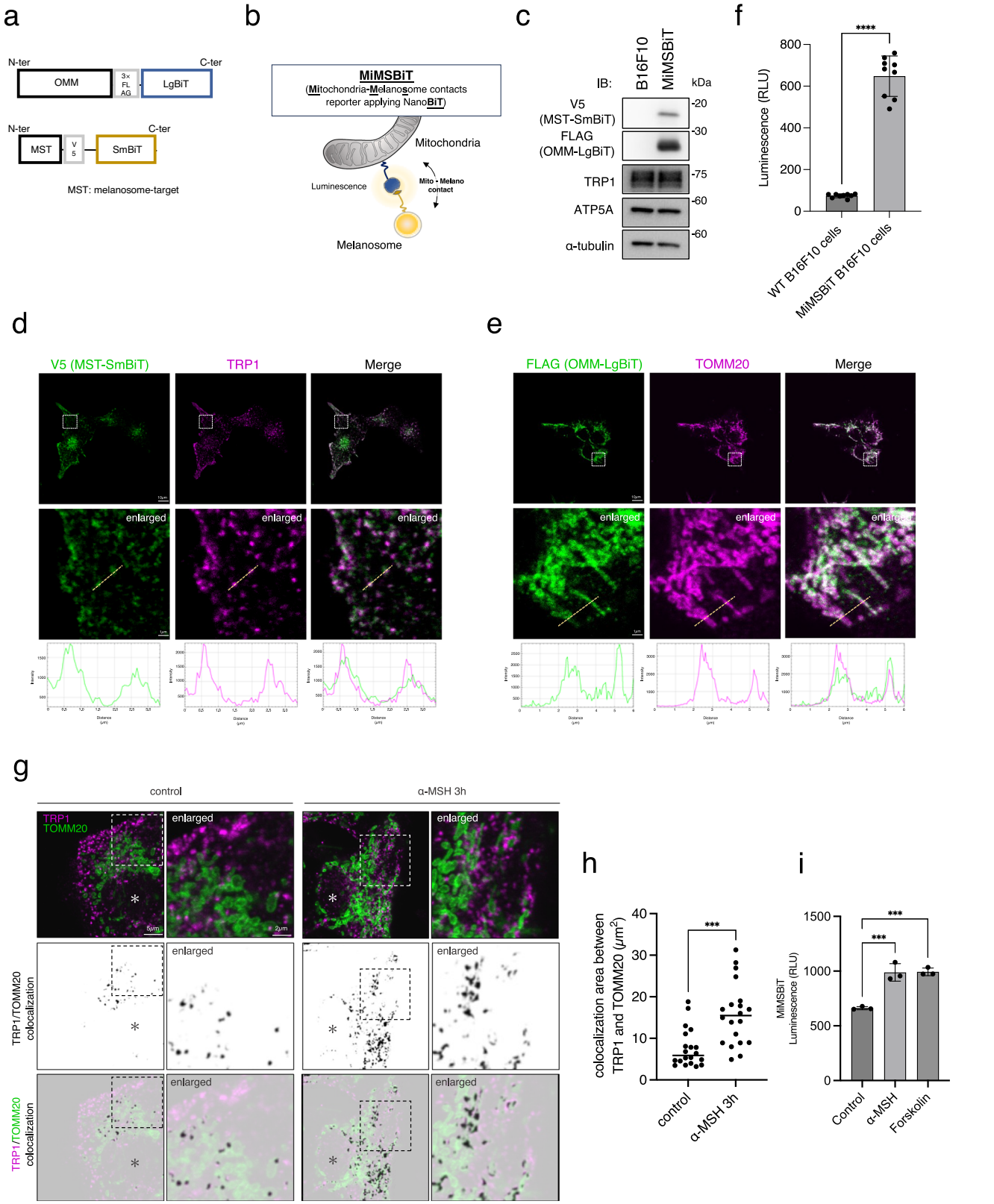

Melanosomes are lysosome-related organelles found in melanocytes and retinal pigment cells, specialized for the synthesis, storage, and transport of melanin[11–14]. They originate from endosomal precursors and undergo a series of maturation stages (I to IV) before facilitating melanin deposition and transport to the cell periphery[15,16]. The synthesis of melanin and the maturation of melanosomes are tightly regulated by secreted hormones, including α-melanocyte-stimulating hormone (α-MSH)[17,18]. Exposure to these hormones or ultraviolet (UV) light triggers signaling pathways, such as the cyclic adenosine monophosphate (cAMP)/protein kinase A (PKA) pathway, which promote melanin production and pigmentation[19–21]. Melanin is synthesized through an enzymatic process catalyzed by tyrosinase, tyrosinase-related protein 1 (Trp1), and dopachrome tautomerase, all of which are localized within the

Fig. 1 | Design of a reversible mitochondria and melanosome contacts quantification assay system – MiMSBiT. a,**b** Schematic of the construct and strategy for detecting mitochondria and melanosome contacts. **c** Representative immunoblots for each component of B16F10 cells and MiMSBiT cells. The lysates were analyzed by immunoblotting for V5, FLAG, TRP1 (melanosome maker), ATP5A (mitochondria maker), and α-tubulin. **d**,**e** Representative images of MST-V5-SmBiT and TOMM20 Nter 1–33aa (OMM)-3×FLAG-LgBiT localization in B16F10 cells stably expressing MST-V5-SmBiT and OMM×FLAG-LgBiT (MiMSBiT cells). Cells were stained with V5, FLAG, TOMM20, and TRP1 antibodies. TOMM20 is used as a mitochondrial marker, and TRP1 is used as a melanosomal marker. Line scans below the images indicate colocalization between V5 or FLAG (green) and melanosome maker TRP1 or mitochondria maker TOMM20 (magenta) and correlate to the lines drawn in the images. **f** Luminescence of MiMSBiT cells. Quantification of the luminescence of B16F10 cells, MiMSBiT cells. Data are mean ± s.e.m. ($n = 9$). **g**,**h** Mitochondria and melanosome contacts increase under α-MSH stimulation. Cells were stimulated with α-MSH for 3 hours. Cells were stained with TOMM20 and TRP1 antibodies. TOMM20 is used as a mitochondrial marker, and TRP1 is used as a melanosomal marker. The colocalization between melanosome and mitochondria extract using ImageJ and the area of colocalization was calculated. Data are mean ± s.e.m. Data from three biological replicates. Number of ROI counted in each experiment: (7, 7, 6). **i** MiMSBiT signals were increased in α-MSH and forskolin stimulation. Cells were treated with α-MSH and forskolin, a PKA activator, then luminescence of MiMSBiT cells were measured. Data are mean ± s.e.m. ($n = 3$, triplicate). Statistical significance was analyzed by one-way analysis of variance (ANOVA) (**i**) or Student's t-test, Two-tailed (**f, h**). P values are indicated as; $^{***}p < 0.001$; $^{****}p < 0.0001$. n indicates independent biological experiments, unless otherwise indicated.

lumen of melanosomes and contribute to pigmentation[22]. Melanosomes are known to modulate the pH of their lumen during the maturation process. De-acidification is required for tyrosinase activation, whereas preceding acidification is essential for PMEL fibrillation, which provides a scaffold for melanin deposition[23]. Notably, protein fibrillation is promoted under acidic conditions[24]. The melanosome fibril protein PMEL was the first natural amyloid described in mammals[25] and forms amyloid fibrils only under the acidic conditions characteristic of the lysosome-like melanosome lumen, facilitating melanin synthesis and deposition[26]. However, the impact of mitochondria-melanosome contact on melanosome lumen pH and PMEL fibrillation remains poorly understood at the molecular and functional levels.

In this study, we utilized the NanoBiT system to measure reversible mitochondria-melanosome contacts in living cells and investigate their physiological role. Our findings reveal that MFN2-STIM1-mediated mitochondria-melanosome contact regulates melanosome lumen acidification, thereby promoting PMEL fibrillation and ensuring proper melanosome maturation.

Results

Assay system for quantifying reversible mitochondria-melanosome contact – MiMSBiT

Organelle contacts are dynamic and play critical physiological roles. However, due to the limitations of existing quantification methods, analyzing the physiological functions of organelle contact dynamics in living cells remains an area for development. In a previous study, we developed a tool to quantify reversible ER-mitochondria contacts in living cells using the NanoBiT system[27]. In this study, we adapted the same system to measure reversible contacts between mitochondria and melanosomes. To achieve this, we generated B16F10 cells stably expressing outer mitochondrial membrane (OMM)-targeting LgBiT (a large fragment of NanoBiT fused to human TOMM20 1-33aa) and melanosome-targeting SmBiT (a small fragment of NanoBiT fused to a melanosome-targeting tag, MST, derived from mouse Mreg 1–139 aa as previously described[28]). This system, named MiMSBiT (Mitochondria-Melanosome contact reporter applying NanoBiT), is illustrated and characterized in Fig. 1a–e. Luminescence was measured in MiMSBiT-expressing cells, and we observed significantly higher luminescence compared to cells that did not express the MiMSBiT system (Fig. 1f). A previous study has suggested that mitochondria and melanosomes exhibit increased contact during the early stages of melanosomal biogenesis[10]. Based on this, we hypothesized that mitochondria-melanosome contacts may also play a functional role during melanosome maturation. Using immunostaining analysis, we observed that α-MSH stimulation increased mitochondria–melanosome contacts (Fig. 1g, h). Consistently, MiMSBiT-based luminescence measurements revealed that stimulation with either α-MSH or forskolin, both of which enhance melanosome maturation, increased mitochondria–melanosome contacts (Fig. 1i). Together, these results demonstrate that the NanoBiT system is a powerful and reliable tool for quantifying mitochondria-melanosome contacts in living cells.

MFN2 as a critical tethering factor for mitochondria-melanosome contacts during melanosome maturation

Mitochondria-melanosome contacts have been reported to be mediated by MFN2 in melanocytes[10]. To determine whether the α-MSH-stimulated contact between mitochondria and melanosomes is regulated by MFN2, we examined the formation of these contacts under conditions of *Mfn2* knockdown, as well as knockdown of other known mitochondrial fission and fusion factors, including Drp1, Opa1, and Mfn1[29]. Our results showed that knockdown of Mfn2 specifically suppressed α-MSH-induced mitochondria-melanosome contact, whereas knockdown of the other factors had no significant effect (Fig. 2a–d). Further investigation revealed that the reduction in α-MSH-dependent mitochondria-melanosome contact caused by *Mfn2* knockdown was rescued by re-expression of wild-type (WT) MFN2, but not by re-expression of GTPase-inactive MFN2 mutants (Fig. 2e). Since MFN2 is known to localize to both mitochondria and the ER[6,30], we investigated whether the α-MSH-stimulated contacts are specifically regulated by mitochondria-localized or ER-localized MFN2. Using mitochondria-targeted and ER-targeted MFN2 constructs, we found that the α-MSH-induced mitochondria-melanosome contact suppressed by *Mfn2* knockdown was restored by re-expression of mitochondria-targeted MFN2, but not by ER-targeted MFN2 (Fig. 2f). These findings demonstrate that α-MSH-stimulated mitochondria-melanosome contacts are specifically regulated by mitochondria-localized MFN2. Next, we investigated the impact of mitochondria-melanosome contact on melanosome pigmentation. Prolonged α-MSH stimulation of B16F10 cells promotes melanin synthesis and pigmentation through melanosome maturation. *Mfn2* knockdown significantly inhibited pigmentation induced by α-MSH stimulation, and this inhibition was rescued by the re-expression of WT MFN2 but not by GTPase-inactive MFN2 mutant (Fig. 2g, h). Melanin synthesis is mediated by tyrosinase, an enzyme localized within melanosomes (Supplementary Fig. 1a–c). To assess the effect of MFN2 on tyrosinase activity, we used bafilomycin A1, a H^+-ATPase inhibitor, which can acutely induce melanosome de-acidification and activate tyrosinase, thereby stimulating acute melanin synthesis (Supplementary Fig. 1b). Our results showed that suppression of *Mfn2* did not alter tyrosinase expression levels (Fig. 2i–k) or the melanin synthesis induced by the acute activation of tyrosinase with bafilomycin A1 (Supplementary Fig. 1d, e). These findings demonstrate that MFN2 activation positively regulates mitochondria-melanosome contact as well as α-MSH-induced pigmentation, while not affecting the expression or activity of tyrosinase.

MFN2 is required for melanosome acidification and PMEL fibrillation

The acidification of the melanosome lumen at precise stages is critical for melanosome maturation. Given that MFN2 does not regulate

https://doi.org/10.1038/s41467-026-70282-w

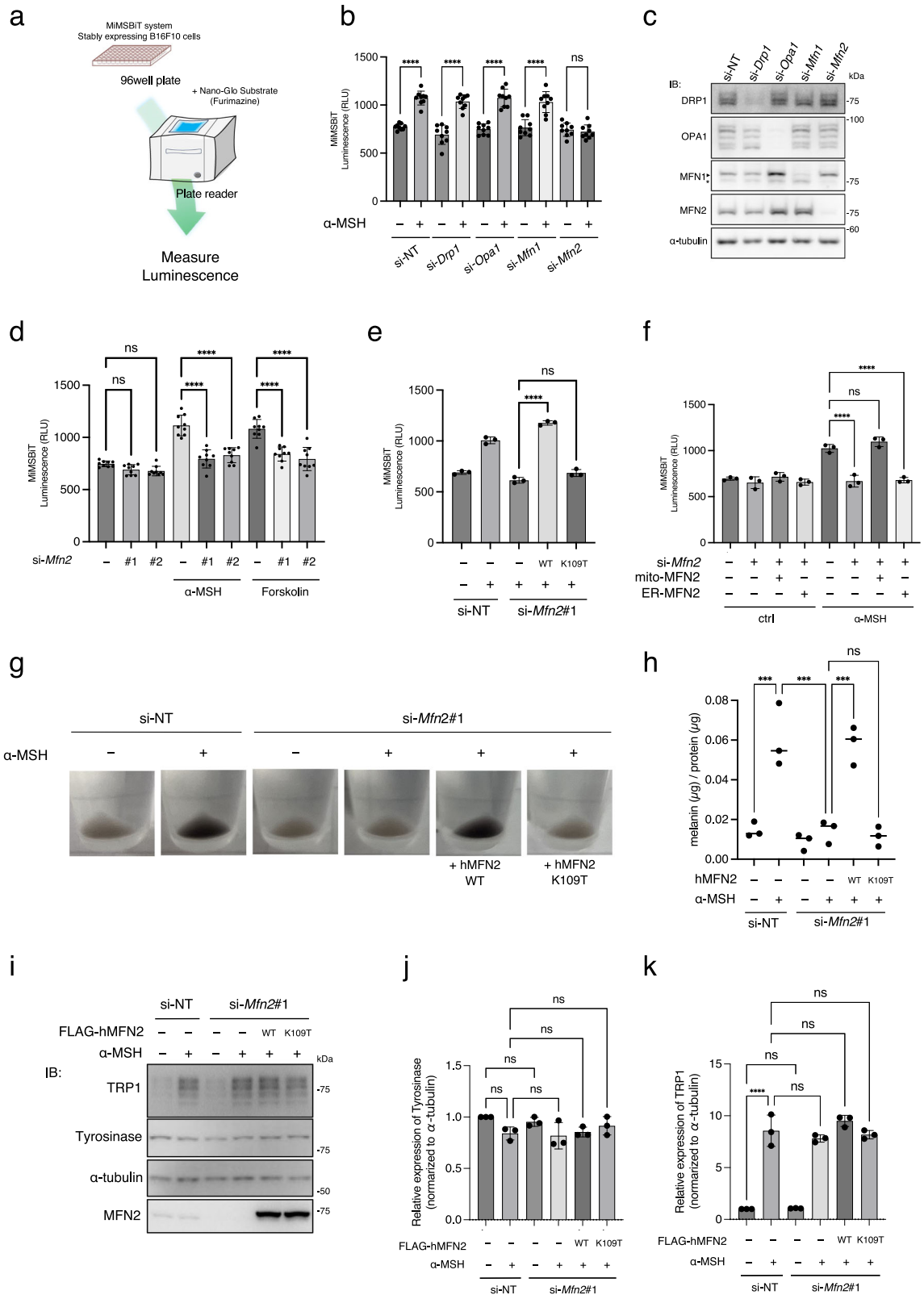

tyrosinase expression or activity, we hypothesized that it may instead influence melanosome acidification during α-MSH-induced maturation. To test this, we used MELOPS, a melanosome-specific pH indicator[31], to measure the pH of the melanosome lumen. Since bafilomycin A1 treatment, which induces melanosome de-acidification via inhibition of V(H⁺)-ATPase, increases MELOPS fluorescence, we confirmed that MELOPS accurately reflects changes in melanosome lumen pH (Supplementary Fig. 2a, b). Using this indicator, we monitored temporal changes in melanosome pH following α-MSH stimulation and observed that melanosome acidification peaked 3 hours after stimulation with α-MSH or forskolin (Fig. 3a, b and Supplementary Fig. 2a, b). To determine whether this α-MSH–dependent acidification was mediated by V(H⁺)-ATPase activity, bafilomycin A1 was added after 3 hours of α-MSH stimulation. Bafilomycin A1 treatment resulted in a

Fig. 2 | MFN2 is essential for mitochondria and melanosome contacts. a–c Effects of suppression for DRP1, OPA1, MFN1, and MFN2 on luminescence in MiMSBiT cells under α-MSH stimulation. Cells were transfected with the indicated siRNAs and then luminescence was measured or WB was performed with the indicated antibodies to confirm protein expression levels. Data are mean ± s.e.m. ($n = 3$, triplicate). **d** MFN2 is critical tethering factor for mitochondria and melanosome contact formation induced by α-MSH and Forskolin stimulation. MiMSBiT cells were transfected with the indicated siRNAs for 3 days and treated with or without α-MSH and Forskolin for 3 h before luminescence measurements. Data are mean ± s.e.m. ($n = 3$, triplicate). **e** MFN2 GTPase activity is indispensable for mitochondria and melanosome contacts formation induced by α-MSH stimulation. The MiMSBiT cells were transfected with the indicated siRNAs for 2 days. Then transfected with empty vectors or indicated RNAi-resistant MFN2 vectors for 1 day. Before measuring luminescence, cells were treated with or without α-MSH for 3 hours. Data are mean ± s.e.m. ($n = 3$, triplicate). **f** Mitochondrial MFN2 not ER MFN2 is indispensable for mitochondria and melanosome contact formation induced by α-MSH stimulation. The MiMSBiT cells were transfected with the indicated siRNAs for 2 days. Then transfected with empty vectors or indicated RNAi-resistant mitochondria or ER targeted MFN2 vectors for 1 day. Before measuring luminescence, cells were treated with or without α-MSH for 3 h. Data are mean ± s.e.m. ($n = 3$, triplicate). **g**,**h** MFN2 GTPase activity is indispensable for pigmentation induced by α-MSH stimulation. The B16F10 cells were transfected with the indicated siRNAs for 2 days. Then transfected with empty vectors or indicated RNAi-resistant MFN2 vectors for 1 day. Before collecting the cell pellet and measuring melanin content, cells were treated with or without α-MSH for 24 h. Data are mean ± s.e.m. ($n = 3$). **i–k** MFN2 does not affect TRP1 and Tyrosinase expression levels under α-MSH stimulation. The B16F10 cells were transfected with the indicated siRNAs for 2 days. Then transfected with empty vectors or indicated RNAi-resistant MFN2 vectors for 1 day. Cells were treated with or without α-MSH for 24 h and WB was performed with the indicated antibodies to confirm protein expression levels and quantified. MFN2 K109T mutant: lack of GTPase activity. Data are mean ± s.e.m. ($n = 3$). Statistical significance was analyzed by one-way analysis of variance (ANOVA) (**b**,**d**,**e**,**f**,**h**,**j**,**k**). P values are indicated as; ***$p < 0.001$; ****$p < 0.0001$; n.s., not significant. n indicates independent biological experiments, unless otherwise indicated.

marked reduction in MELOPS fluorescence. These results indicate that α-MSH–induced melanosome acidification is largely dependent on V(H^+)-ATPase activity. Notably, the peak in melanosome acidification coincided with the highest luminescence detected by the MiMSBiT system, observed 3 hours after α-MSH stimulation (Fig. 3c and Supplementary Fig. 2c). Depletion of *Mfn2* inhibited the α-MSH-dependent acidification of the melanosome lumen, and this inhibition was rescued by re-expression of WT MFN2 but not by GTPase-inactive MFN2 mutants (Fig. 3a, b and Supplementary Fig. 2d). To further investigate the role of MFN2 in melanosome maturation, we examined its effect on melanosome acidification and PMEL fibrillation. During melanosome maturation, PMEL undergoes cleavage to form fibrils that serve as a scaffold for melanin deposition (Fig. 3d). It is well established that the fibrillation of PMEL is promoted by the acidification of the melanosome lumen. Using PMEL fibril-specific antibodies, we observed that fibrillation peaked around 3 h after α-MSH stimulation, coinciding with the peak in acidification and mitochondria-melanosome contact (Fig. 3e, Supplementary Fig. 2e, f). Furthermore, inhibition of *Mfn2* suppressed PMEL fibrillation following 3 hours of α-MSH stimulation (Fig. 3f). These findings suggest that MFN2 promotes mitochondria-melanosome contact, thereby facilitating melanosome acidification and enhancing PMEL fibrillation during maturation.

STIM1 binds to MFN2 and functions as a tethering factor for mitochondria-melanosome contacts

Figure 2f clearly shows that mitochondria-localized MFN2 is crucial for mitochondria-melanosome contact. However, the tethering factor on the melanosome side remains unclear. To identify the melanosome-localized tethering factor interacting with MFN2, we utilized the TurboID proximal biotin labeling approach[32]. Given the propensity of TurboID for non-specific labeling, the identified proteins were considered potential interactors. By conjugating TurboID to MFN2, we analyzed proteins potentially in close proximity to MFN2 under α-MSH stimulation for 3 h, a time point when mitochondria-melanosome contact is maximally increased (Fig. 4a–d). This approach facilitated the identification of proteins biotinylated by TurboID in close proximity through quantitative proteomics based on mass spectrometry (Fig. 4d, Supplementary Fig. 3a–c, Supplementary Data 1). Among these potential interactors, we focused on STIM1, a protein previously known not to localize to mitochondria (Fig. 4d, Supplementary Fig. 3a–c). While STIM1 is widely recognized as an ER-localized protein, our immunostaining analysis revealed that it co-localizes with TRP1, a melanosome marker, in B16F10 cells (Fig. 4e, f). Further immunoprecipitation analysis showed that STIM1 transiently binds to MFN2 at 3 h after α-MSH stimulation but dissociates by 12 h (Fig. 4g). Additionally, knockdown of *Stim1* significantly reduced α-MSH-dependent mitochondria-melanosome contacts (Fig. 4h). These results suggest that melanosome-localized STIM1 interacts with mitochondrial MFN2 to promote mitochondria-melanosome contacts during melanosome maturation.

STIM1 binds to MFN2 in response to calcium depletion and is essential for melanosome acidification and PMEL fibrillation

Since STIM1 has been shown to bind to MFN2 and regulate mitochondria-melanosome contact, we analyzed the role of STIM1 in melanosome maturation alongside MFN2. Similar to the effects observed for MFN2 suppression, *Stim1* knockdown inhibited α-MSH-stimulated melanosome acidification, melanogenesis, and PMEL fibrillation (Fig. 5a–d). To further evaluate the effects of STIM1 and MFN2 on melanosome maturation and mitochondria–melanosome contact, we performed electron microscopy analysis. Following 3 hours of α-MSH stimulation, the number of fibril-containing melanosomes was increased in control cells, whereas this increase was significantly suppressed by knockdown of MFN2 or STIM1 (Fig. 5e, f). Consistently, the number of mitochondria–melanosome contacts was also reduced in *Mfn2* or *Stim1* knockdown cells (Supplementary Fig. 3d). While STIM1 clearly binds to MFN2 in an α-MSH-dependent manner, the mechanism regulating this interaction remains unclear. STIM1 contains a calcium-binding domain and functions as a calcium sensor. When calcium levels decrease, calcium dissociation from STIM1 calcium-binding domain induces STIM1 clustering. We hypothesized that STIM1 binds to MFN2 through clustering triggered by α-MSH stimulation. To test this, we used BN-PAGE to analyze whether MFN2-STIM1 forms a protein complex and found that MFN2 associates with STIM1 in a large complex in an α-MSH-dependent manner (Fig. 5g). Furthermore, treatment with the calcium chelator BAPTA-AM enhanced MFN2-STIM1 binding and increased mitochondria-melanosome contact (Fig. 5h, i). To further investigate the relationship between calcium levels and contact formation, we targeted the calcium indicator RCaMP to the melanosome lumen (Supplementary Fig. 3e). Using melanosome-targeted RCaMP under α-MSH stimulation, we observed a significant decrease in melanosomal calcium concentration 30 minutes after stimulation (Fig. 5j, k). These findings demonstrate that STIM1 facilitates MFN2 binding by clustering in response to calcium depletion in the melanosome lumen, thereby promoting mitochondria-melanosome contact during melanosome maturation.

Mitochondrial ATP production facilitates melanosome acidification and PMEL fibrillation

While STIM1-MFN2 binding increases mitochondria-melanosome contacts in an α-MSH-dependent manner, the physiological

https://doi.org/10.1038/s41467-026-70282-w

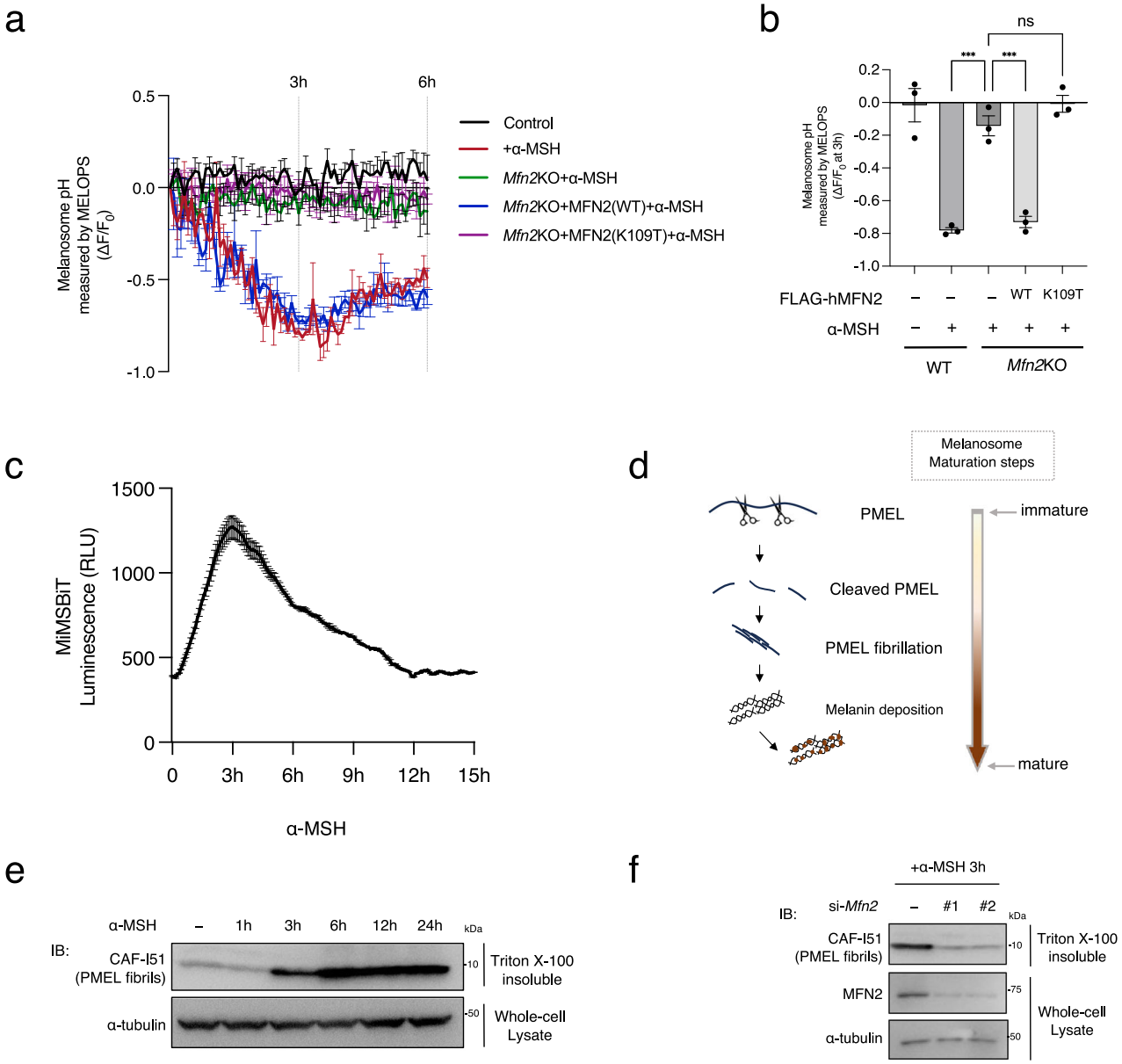

Fig. 3 | Melanosomal matrix pH and PMEL fibrillation were regulated by MFN2. **a**,**b** MFN2 and its GTPase activity are indispensable for melanosomal acidification induced by α-MSH stimulation. *MFN2* knockout (KO) B16F10 cells were transfected with the indicated constructs, and stably expressing cells were selected by puromycin selection. The cells were then transfected with melanosome matrix–targeted MELOPS and stimulated with α-MSH. MELOPS fluorescence was subsequently measured kinetically at 5-min intervals using a plate reader. Figure 3b shows quantification of the data in the Fig. 3a at 3 h of stimulation with α-MSH. Data are mean ± s.e.m. ($n = 3$). **c** Melanosome and mitochondria contact dynamics under α-MSH stimulation. MiMSBiT cells were treated with α-MSH and subsequently measured luminescence kinetically at 5 min intervals using a plate reader. Data are mean ± s.e.m. ($n = 3$). **d**,**e** PMEL fibrillation under α-MSH stimulation. The B16F10 cells were treated with α-MSH indicated times and then isolated 1% Triton X-100 insoluble pellet by sedimentation. The pellet was re-extracted with 1% SDS containing buffer (Triton X-100 insoluble fraction). WB was performed with the indicated antibodies to confirm protein expression levels. **f** MFN2 regulates PMEL fibrillation under α-MSH stimulation. The B16F10 cells were transfected with the indicated siRNAs for 2 days. Then, treated with α-MSH for 3 hours, and isolated 1% Triton X-100 insoluble pellet by sedimentation. The pellet was re-extracted with 1% SDS containing buffer (Triton X-100 insoluble fraction). WB was performed with the indicated antibodies to confirm protein expression levels. Statistical significance was analyzed by one-way analysis of variance (ANOVA) (**b**). P values are indicated as; $^{***}p < 0.001$; n.s., not significant. n indicates independent biological experiments, unless otherwise indicated.

consequences of these contacts remained to be determined. As an initial analysis, we found that melanosome pigmentation was suppressed when mitochondrial ATP synthesis was inhibited using oligomycin, a mitochondrial Complex V inhibitor (Fig. 6a, b). Further analysis showed that oligomycin treatment suppressed α-MSH-dependent melanosome acidification and PMEL fibrillation (Fig. 6c–e) without altering TRP1 or tyrosinase expression levels (Fig. 6f–h). Moreover, pigmentation induced by bafilomycin A1 was not suppressed by oligomycin treatment, indicating that bafilomycin A1–induced pigmentation is not dependent on mitochondrial ATP production (Fig. 6i, j). These findings demonstrate that mitochondrial ATP production is crucial for facilitating melanosome acidification and PMEL fibrillation during maturation.

Consistent with these results, mitochondrial ATP production is essential for pigmentation. Acidification of the melanosome lumen is regulated by V(H^+)-ATPase, an ATP-driven proton pump localized on the melanosome membrane[33]. Based on this, we hypothesized that mitochondria supply ATP to melanosomes through direct contact,

https://doi.org/10.1038/s41467-026-70282-w

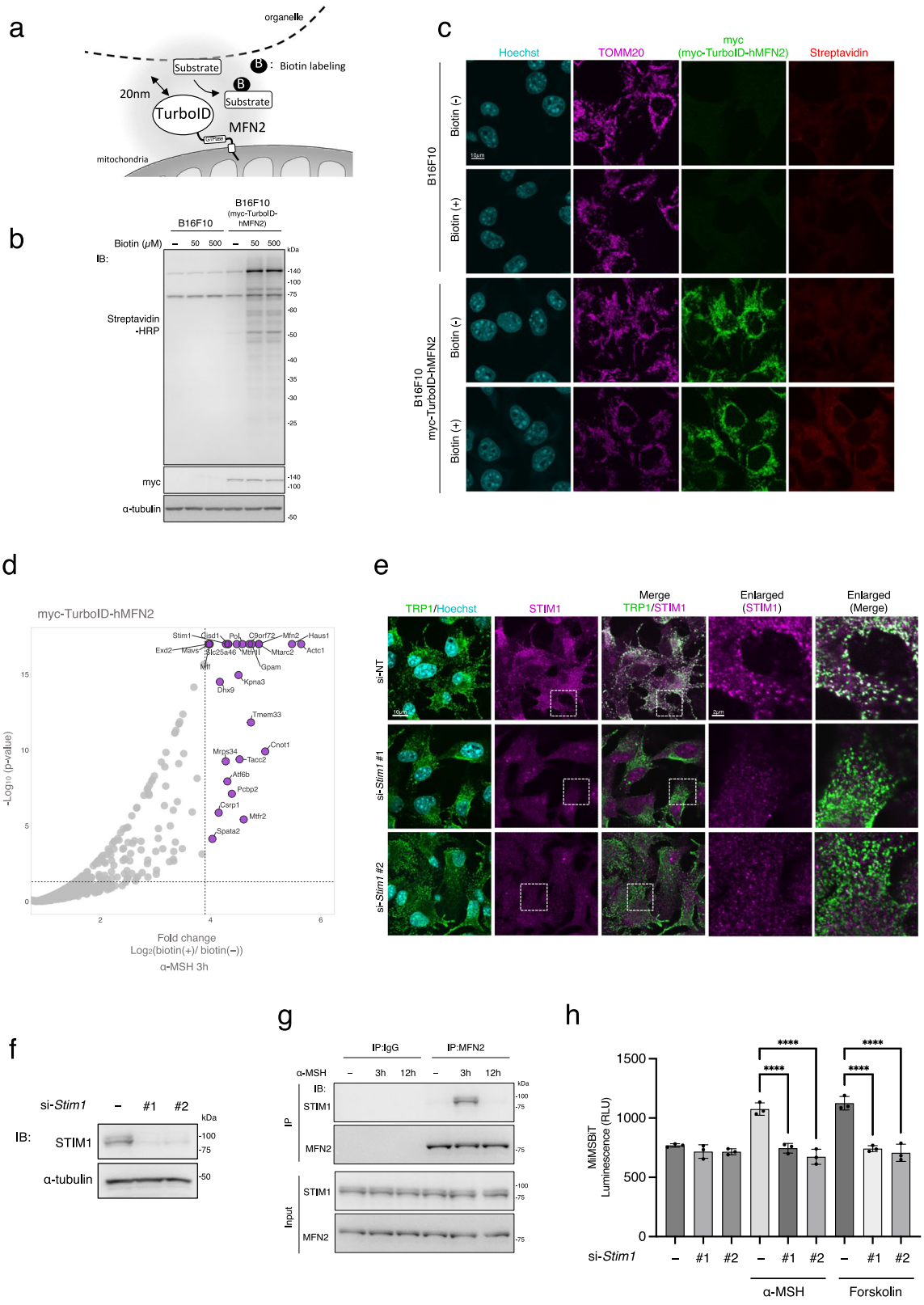

transiently activating V(H$^+$)-ATPase and promoting acidification. To investigate how ATP concentration around melanosomes changes during contact with mitochondria, we targeted the ATP-sensing fluorescent protein iATPSnFR2[34] to the cytoplasmic side of the melanosome membrane (Supplementary Fig. 3f). Cellular ATP production occurs via two main pathways: glycolysis in the cytoplasm and oxidative phosphorylation (OXPHOS) in mitochondria. To determine which pathway contributes to ATP levels around melanosomes, we analyzed the fluorescence intensity of melanosome-localized iATPSnFR2 under conditions with or without treatment with 2-deoxy-D-glucose (2-DG), an inhibitor of hexokinase, the rate-limiting enzyme in glycolysis (Fig. 7a–e). An α-MSH–dependent increase in iATPSnFR2 fluorescence was observed even in the absence of 2-DG treatment and was suppressed by oligomycin (Fig. 7b, c). A similar pattern of α-

Fig. 4 | STIM1 localizes melanosome and interacts with MFN2 to tether mitochondria and melanosome contacts under α-MSH stimulation. a–c Generation of B16F10 cells stably expressing myc-TurboID-MFN2. The B16F10 cells stably expressing myc-TurboID-MFN2 were treated with biotin indicated concentration for 15 min. Then, WB and immunofluorescence were performed with the indicated antibodies to confirm protein expression levels and localization. **d** A volcano plot showing biotinylated proteins by TurboID-MFN2 after α-MSH stimulation for 3 h. Biotinylated proteins enriched by pull-down were identified and quantified with mass spectrometry-based proteomic analysis and label-free quantification (LFQ). The x-axis represents the logarithm of a ratio of protein abundances in the biotin-treated and biotin-untreated samples (base: 2), and the y-axis denotes a represents a logarithm of a p-value. The top 25 proteins with the highest abundance ratio ($p \leq 0.05$) were marked with their gene names. **e**,**f** STIM1 localizes melanosome. The B16F10 cells were transfected with the indicated siRNAs for 2 days. Then, immunostaining and WB analysis were performed indicating antibodies. TRP1 is used as a melanosomal marker. **g** STIM1 interacts with MFN2 in the early stages of α-MSH stimulation. The B16F10 cells were treated with α-MSH indicated time. Then, cell lysates were subjected to IP assay with anti-MFN2 antibody and IB assay with the indicated antibodies. **h** STIM1 is critical tethering factor for mitochondria and melanosome contacts formation induced by α-MSH and Forskolin stimulation. MiMSBiT cells were transfected with the indicated siRNAs for 3 days and treated with or without α-MSH and Forskolin for 3 h before luminescence measurements. Data are mean ± s.e.m. ($n = 3$, triplicate). Statistical significance was analyzed by one-way analysis of variance (ANOVA) (**h**). P values are indicated as; ****$p < 0.0001$. Statistical analysis for the proteomics data shown in (**d**) was performed using Proteome Discoverer. Differential protein abundance was assessed using a background-based t-test implemented in the software. n indicates independent biological experiments, unless otherwise indicated.

MSH–dependent signal increase and oligomycin sensitivity was also observed in the presence of 2-DG, indicating that the ATP increase around melanosomes upon α-MSH stimulation is largely derived from mitochondrial OXPHOS (Fig. 7d, e). Notably, neither 2-DG nor oligomycin treatment significantly affected mitochondria–melanosome contact (Fig. 7f). To confirm whether mitochondria-derived ATP concentration around melanosomes is regulated by mitochondria–melanosome contact, we performed knockdown of *Mfn2* or *Stim1* in the presence or absence of 2-DG and measured mitochondria-derived ATP levels around melanosomes. In both conditions, depletion of *Mfn2* or *Stim1* significantly reduced the α-MSH–induced increase in mitochondria-derived ATP concentration around melanosomes (Fig. 7g–j). These findings suggest that melanosomes establish contact with mitochondria in response to α-MSH stimulation. At MFN2-STIM1-mediated contact sites, melanosomes are likely exposed to a locally high concentration of mitochondria-derived ATP, possibly where V(H^+)-ATPase co-localizes, thereby promoting melanosome acidification.

MFN2–STIM1 interaction is required for melanosome maturation and pigmentation in vivo

To identify the domain of MFN2 required for its interaction with STIM1, we focused on the heptad repeat domains HR1 and HR2 of MFN2. Analysis of deletion mutants revealed that MFN2 lacking the HR2 domain, but not HR1, significantly attenuated the α-MSH–dependent binding of MFN2 to STIM1 (Fig. 8a). Consistently, treatment with a previously characterized mitofusin inhibitor[35] that targets the HR2 domain of MFN2 also markedly reduced the interaction between MFN2 and STIM1 (Fig. 8b). These results indicate that the HR2 domain of MFN2 is critical for its interaction with STIM1. Furthermore, inhibition of mitofusin HR2 function significantly suppressed α-MSH–dependent acidification of the melanosome lumen (Fig. 8c, d), supporting a functional link between MFN2–STIM1 binding and melanosome maturation. To examine the physiological significance of MFN2–STIM1–mediated mitochondria–melanosome contact at the in vivo level, we analyzed pigmentation in zebrafish, in which melanization is known to be regulated by α-MSH[36]. Treatment of zebrafish embryos with the mitofusin inhibitor at early developmental stages resulted in a marked reduction in body pigmentation compared with control embryos (Fig. 8e, f). These findings suggest that MFN2–STIM1 interaction is required for α-MSH–dependent melanization in vivo.

Discussion

Mitochondria-melanosome interactions regulate melanosome maturation

Organelle-organelle interactions play a pivotal role in coordinating intracellular functions. Here, we developed a reversible mitochondria-melanosome contact measurement system (MiMSBiT) in living cells, allowing us to uncover a dynamic, calcium-regulated interaction between these organelles in response to α-MSH stimulation. Our findings reveal that mitochondria-melanosome contacts transiently increase upon α-MSH stimulation, followed by a gradual decline, highlighting the tightly regulated nature of this process (Fig. 8g).

By employing TurboID-MFN2-based proximity labeling, we identified STIM1 as a key regulator of these interactions. While STIM1 is well known as an ER-localized calcium sensor, our data demonstrate that STIM1 localizes to melanosomes in B16F10 melanoma cells, where it forms a complex with MFN2 in response to α-MSH-induced calcium depletion within the melanosomal lumen. Notably, STIM1 clustering is essential for mitochondria-melanosome contact formation, supporting a model in which calcium-dependent STIM1 reorganization facilitates inter-organelle tethering. Given that STIM1 senses ER luminal calcium depletion and facilitates store-operated calcium entry via Orai1 at the plasma membrane[37], our findings suggest that STIM1 plays a similar calcium-sensing role in melanosomes, linking mitochondrial function to calcium homeostasis in these organelles.

Mechanisms underlying organelle detachment and calcium regulation

While the precise mechanism underlying organelle detachment remains unclear, we observed that MFN2-STIM1 interactions are progressively lost in the later stages of α-MSH stimulation, suggesting a regulated disassembly process. Given that SLC25A4, a mitochondrial and melanosomal calcium transporter, is crucial for melanosomal calcium accumulation and PMEL fibril formation[38,39], mitochondrial calcium efflux via SLC25A4 may contribute to the disengagement of these organelles. Furthermore, TPC2, another calcium transporter, has been shown to regulate melanosomal calcium concentration[31], raising the possibility that coordinated activity of TPC2 and SLC25A4 may establish a calcium gradient that controls organelle attachment and detachment. Since STIM1 undergoes structural rearrangements and oligomerization in response to calcium depletion in the ER[37], future studies should address whether STIM1 undergoes a similar conformational change in melanosomes that regulates its affinity for MFN2.

Physiological significance of mitochondria-melanosome interactions

Functionally, mitochondria-melanosome contacts appear to provide localized sites of ATP utilization, which in turn activate V(H^+)-ATPase on the melanosomal membrane, promoting acidification of the melanosomal lumen. This acidification enhances PMEL fibril formation, a critical step in melanin deposition. Given that PMEL-knockout mice exhibit coat color abnormalities[40] and that mutations in BACE2, a PMEL-processing enzyme, also disrupt pigmentation[41], our findings suggest that regulated PMEL fibril assembly via mitochondria-melanosome crosstalk is essential for proper melanin deposition.

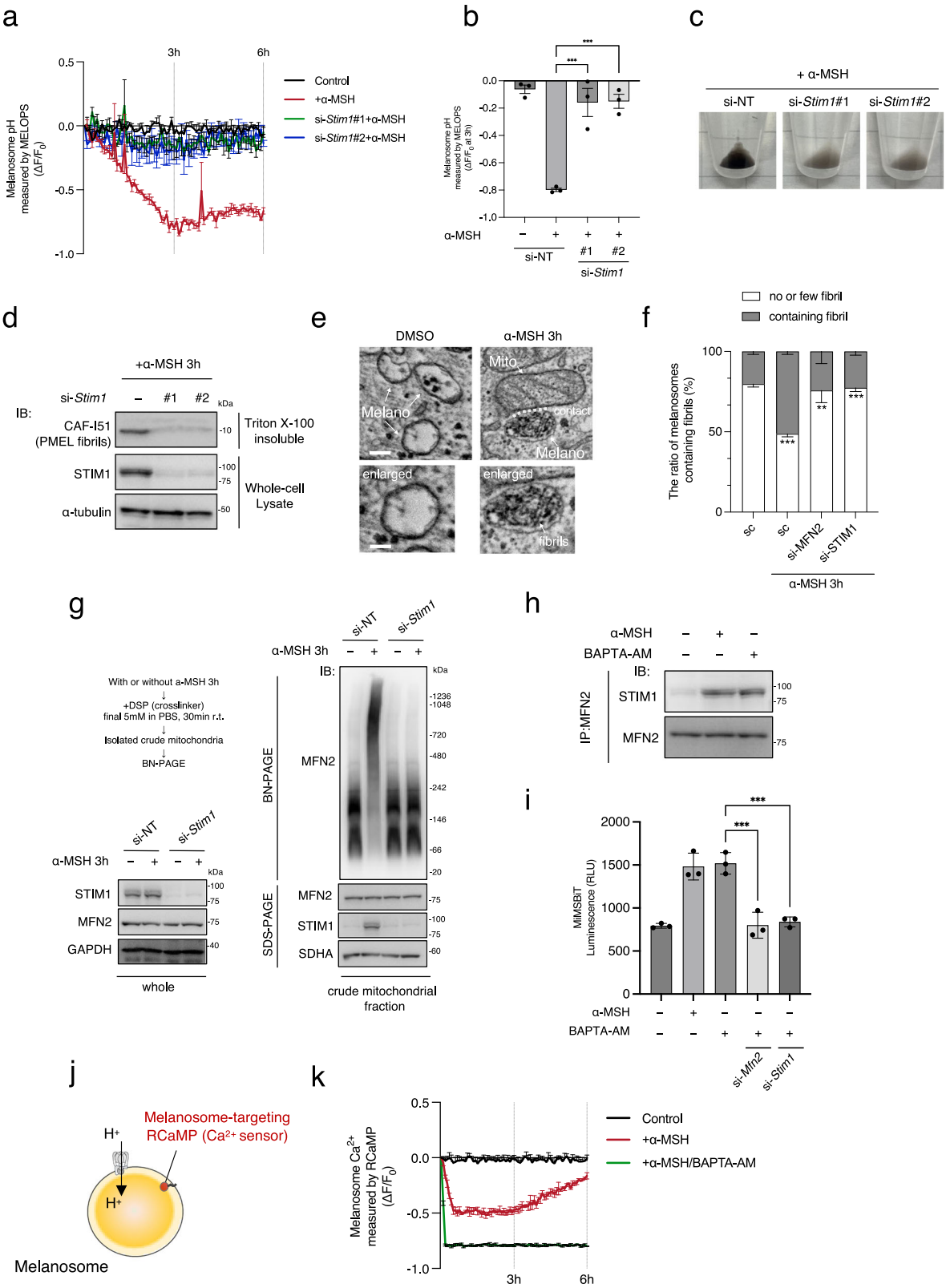

Consistent with our in vitro results, our zebrafish data extend these findings to an in vivo context. Pharmacological inhibition of mitofusin activity in zebrafish embryos resulted in a marked suppression of body pigmentation, indicating that MFN2-dependent mechanisms contribute to melanization at the organismal level. Because zebrafish pigmentation is regulated by α-MSH signaling, these results support the idea that MFN2–STIM1–mediated mitochondria–melanosome interactions represent a conserved regulatory axis linking hormonal stimulation to melanosome maturation in vivo.

Beyond melanogenesis, STIM1 deficiency in zebrafish results in depigmentation[42], suggesting that calcium-mediated inter-organelle communication is broadly relevant to pigmentation biology.

Notably, STIM1 is known to localize to multiple subcellular compartments, and previous work has demonstrated that the

Fig. 5 | STIM1-MFN2 interaction trigged by melanosomal matrix calcium loss regulates melanosomal matrix pH and PMEL fibrillation. a,**b** STIM1 regulates melanosomal matrix pH under α-MSH stimulation. B16F10 cells were transfected with the indicated siRNAs for 2 days, followed by transfection with melanosome matrix–targeted MELOPS for 1 day. Cells were then stimulated with or without α-MSH, and MELOPS fluorescence was monitored kinetically at 5-min intervals using a plate reader. Data are presented as mean ± s.e.m. ($n = 3$). Figure 5b shows quantification of the data shown in Fig. 5a after 3 h of α-MSH stimulation. **c** STIM1 is indispensable for pigmentation induced by α-MSH stimulation. The B16F10 cells were transfected with the indicated siRNAs for 2 days. Before collecting the cell pellet, cells were treated with or without α-MSH for 24 h. **d** STIM1 regulates PMEL fibrillation under α-MSH stimulation. The B16F10 cells were treated with α-MSH for 3 h and then isolated 1% Triton X-100 insoluble pellet by sedimentation. The pellet was re-extracted with 1% SDS containing buffer (Triton X-100 insoluble fraction). WB was performed with the indicated antibodies to confirm protein expression levels. **e**,**f** Melanosomes with fibril formation analyzed by electron microscopy. **e** shows representative electron micrographs of control (si-NT) MNT1 cells stimulated with α-MSH for 3 h. Mito, mitochondria; melano, melanosome. Mitochondria–melanosome contact sites are indicated by dashed white lines (< 25 nm distance between membranes). Scale bars, 250 nm (upper panels) and 166 nm (lower panels). **f** shows quantification of the number of fibril-containing melanosomes in MNT1 cells transfected with control (si-NT), MFN2, or STIM1 siRNAs and stimulated with α-MSH for 3 h. Data are presented as mean ± s.e.m. ($n = 10$ cells per condition). **g** MFN2 assembles a large complex with STIM1 under α-MSH stimulation. The B16F10 cells were transfected with the indicated siRNAs for 2 days. Before collecting the cells, cells were treated with or without α-MSH for 3 h. Then, cells were resuspended with 5 mM DSP, a cross-linker, containing buffer for 30 min and isolated crude mitochondria. BN-PAGE and SDS-PAGE were performed with the indicated antibodies to confirm protein expression levels. **h** Calcium chelate triggers STIM1 and MFN2 interaction. The B16F10 cells were treated with α-MSH or BAPTA-AM (Calcium chelator) for 3 h. Then, cell lysates were subjected to IP assay with anti-MFN2 antibody and IB assay with the indicated antibodies. **i**, Calcium chelate triggers mitochondria-melanosome contacts via STIM1-MFN2 tethering. MiMSBiT cells were transfected with the indicated siRNAs for 2 days and treated with or without α-MSH or BAPTA-AM for 3 h before luminescence measurements. Data are mean ± s.e.m. ($n = 3$, triplicate). **j**,**k** Melanosomal matrix calcium decreases under α-MSH stimulation. B16F10 cells were transfected with melanosome matrix–targeted RCaMP, a calcium indicator, and treated with or without BAPTA-AM for 3 h or stimulated with α-MSH for the indicated times. RCaMP fluorescence was monitored kinetically at 5-min intervals using a plate reader. In Fig. 5k, data are presented as mean ± s.e.m. ($n = 3$). Statistical significance was analyzed by one-way analysis of variance (ANOVA) (**b**,**f**,**i**). P values are indicated as; $^{**}p < 0.01$; $^{***}p < 0.001$. n indicates independent biological experiments, unless otherwise indicated.

STIM1–Orai1 signaling axis is related to pigmentation in vivo[39]. These observations raise the possibility that STIM1 exerts distinct, compartment-specific functions in melanocytes. In this context, our identification of a melanosome-localized pool of STIM1 suggests that STIM1 may coordinate multiple calcium-dependent pathways to regulate pigmentation. Further studies will be required to dissect the relative contributions and regulatory mechanisms of melanosome-localized STIM1 versus STIM1 acting through canonical STIM1–Orai1 signaling. Moreover, mitochondria-organelle interactions are increasingly recognized as crucial regulators of cellular stress responses, bioenergetics, and metabolic homeostasis. It is thus conceivable that mitochondria-melanosome crosstalk may also influence redox homeostasis, autophagy, or intracellular signaling pathways, warranting further investigation.

Future perspectives

Our study establishes mitochondria-melanosome contacts as a previously unrecognized regulatory mechanism in melanosome maturation, yet several fundamental questions remain unanswered. As much of this study was conducted in cultured cells, it is essential to extend these findings to in vivo models to elucidate their physiological significance. In support of this idea, our zebrafish experiments provide initial in vivo evidence that disruption of MFN2 function impairs pigmentation. However, pharmacological inhibition has inherent limitations, and future studies employing genetic approaches will be required to rigorously define the role of MFN2–STIM1 interactions in melanocytes in vivo. A critical next step will be to generate melanocyte-specific *Mfn2* or *Stim1* knockout mice and determine whether these animals exhibit defects in melanin synthesis. Such models will enable assessment of whether mitochondria-melanosome interactions are required for proper pigmentation in a whole-organism context.

Another important question is how mitochondria-melanosome contacts respond to extracellular cues and cellular stress conditions, such as UV irradiation, oxidative stress, or metabolic fluctuations. Given that mitochondria are central hubs for metabolic regulation and stress adaptation, it is conceivable that melanosome function may be tightly linked to mitochondrial metabolic state. Live-cell imaging combined with high-resolution calcium sensors will be instrumental in dissecting the spatiotemporal regulation of mitochondria-melanosome crosstalk under physiological and stress conditions.

Furthermore, it remains to be investigated whether post-translational modifications of MFN2 contribute to its function in mitochondria-melanosome contact formation. Previous studies have shown that MITOL (also known as MARCHF5), a mitochondrial ubiquitin ligase, can ubiquitinate MFN2, thereby modulating its activity in mitochondrial tethering[43]. Although our current data do not directly address this mechanism, future work will examine whether MITOL-mediated ubiquitination influences MFN2's role in mitochondrial-melanosome contacts.

Together, our findings reveal a novel inter-organelle communication axis that regulates melanosome maturation via mitochondrial calcium dynamics, expanding our understanding of how mitochondrial function integrates with intracellular organelle networks to maintain cellular homeostasis.

Methods

All animal experiments were conducted in accordance with relevant ethical regulations and were approved by the Kanazawa University Animal Experiment Committee (protocol no. AP25-084).

Cell Culture and Transfections

B16F10 and MNT1 cells were cultured in Dulbecco's Modified Eagle's Medium (DMEM) with high glucose, supplemented with 10% fetal bovine serum (FBS). Cells were transfected with plasmids using FuGENE HD Transfection Reagent (Promega) or with siRNAs using Lipofectamine RNAiMAX Transfection Reagent (Invitrogen), according to the manufacturer's instructions.

Small Interfering RNA

Knockdown of endogenous mouse *Drp1*, *Opa1*, *Mfn1*, Mfn2, *tyrosinase*, and *Stim1* was performed using the siRNAs that were transfected with Lipofectamin RNAiMAX Transfection Reagent. Nontargeting siRNA (ID:1027281), siRNA targeting mouse *Mfn1* (Catalog No: SI01304387), siRNA targeting mouse *Opa1* (Catalog No: SI01365721), siRNA targeting mouse *Drp1* (Catalog No: SI00982226), siRNA targeting mouse *Stim1* #1 (Catalog No: SI02710736), siRNA targeting mouse *Stim1* #2 (Catalog No:02735068), siRNA targeting mouse *Tmem33* (Catalog No: SI01451366), siRNA targeting mouse *Mff* (Catalog No: SI00855932), and siRNA targeting mouse *tyrosinase* (Catalog No:02739107) were purchased from Qiagen. siRNA targeting human STIM1 (Catalog No: SI04251709) was purchased from Qiagen. Custom-synthesized siRNA

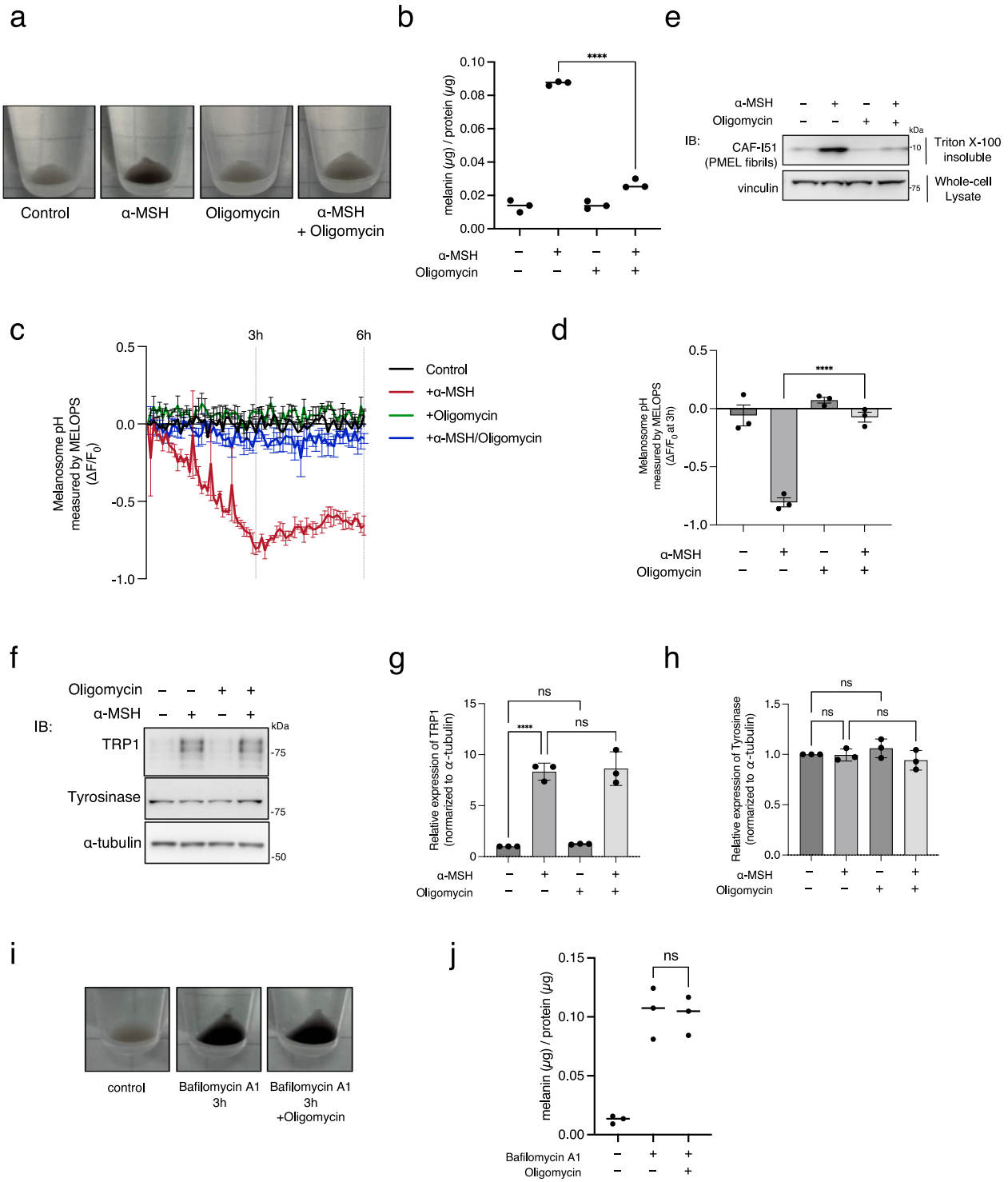

targeting mouse *Mfn2*: sense, 5′-UCCUCAAGGUUUAUAAGAA-3′; human MFN2: 5′-AATCCCAGAGGGCAGAACTTTGTCC-3′[44] were purchased from Japan Bio Services.

Generation of MFN2 knockout cells

To generate mMFN2L-knockout B16F10 cells, CRISPR–Cas9 vectors were constructed. Single-guide RNAs (sgRNAs) targeting the mouse *Mfn2* gene were designed using the online tool CRISPOR. The oligonucleotide pair corresponding to the m*Mfn2* guide RNA (g3: 5′-ACAGGTACCCTTTGACGTCC-3′) was annealed and ligated into the PX459 vector (Addgene plasmid #48139). B16F10 cells were transfected using Lipofectamine 3000 (Invitrogen), and KO clones were selected by serial dilution.

Plasmids and Reagents

To generate stably expressing MiMSBiT system cells, an all-in-one pT4/HB-MiMS vector, including the OMM-targeting LgBiT, melanosome-targeting SmBiT, and IRES-PuroR, was constructed in the optimized Sleeping Beauty transposon vector (Addgene #108352)[45]. The OMM-targeting LgBiT was fused to an N-terminal human TOMM20 (1-33 aa)

Fig. 6 | Mitochondrial ATP production is necessary for acidification of melanosome and PMEL fibrillation. a,**b** Mitochondrial ATP production is indispensable for pigmentation induced by α-MSH stimulation. Before collecting the cell pellet and measuring melanin content, cells were treated with or without α-MSH 24 h and oligomycin every 6 h. Data are mean ± s.e.m. ($n = 3$). **c**,**d** Mitochondrial ATP production is indispensable for melanosomal acidification induced by α-MSH stimulation. B16F10 cells were transfected with melanosome matrix–targeted MELOPS, a pH indicator, for 1 day. Cells were then treated with or without α-MSH and oligomycin, and MELOPS fluorescence was monitored kinetically at 5-min intervals using a plate reader. Figure 6d shows quantification of the data shown in Fig. 6c after 3 h of stimulation. Data are presented as mean ± s.e.m. ($n = 3$). **e** PMEL fibrillation is regulated by mitochondrial ATP production. The B16F10 cells were treated with or without α-MSH and oligomycin for 3 h and then isolated 1% Triton X-100 insoluble pellet by sedimentation. The pellet was re-extracted with 1% SDS containing buffer (Triton X-100 insoluble fraction). WB was performed with the indicated antibodies to confirm protein expression levels. **f**–**h** Mitochondrial ATP production does not affect TRP1 and Tyrosinase expression levels under α-MSH stimulation. The B16F10 cells were treated with or without α-MSH and oligomycin for 3 h and WB was performed with the indicated antibodies to confirm protein expression levels and quantified. Data are mean ± s.e.m. ($n = 3$). **i**,**j** Mitochondrial ATP production does not affect bafilomycin A1 inducible pigmentation. Before collecting the cell pellet and measuring melanin content, cells were treated with or without bafilomycin A1 and oligomycin for 3 h. Data are mean ± s.e.m. ($n = 3$). Statistical significance was analyzed by one-way analysis of variance (ANOVA) (**b**,**d**,**g**,**h**,**j**). P values are indicated as; $^{***}p < 0.001$; $^{****}p < 0.0001$; n.s., not significant. n indicates independent biological experiments, unless otherwise indicated.

and a 3xFLAG-tag and was expressed under the EF-1α promoter. The melanosome-targeting SmBiT was fused to an N-terminal MST-tag (mouse Mreg 1-139 aa), as previously described[28], and a V5-tag, and was expressed under the CBh promoter along with PuroR. To generate stably expressing myc-TurboID-MFN2 cells, myc-TurboID-MFN2 were subcloned into the pCX4 retroviral vector[46]. The localization-restricted Mfn2, mitochondrial Mfn2 (Mfn2ActA) and ER Mfn2 (Mfn2IYFFT) were constructed as previously reported[43]. Human MFN2 deletion mutants lacking the HR1 (Δ371–441) or HR2 (Δ693–747) domains were generated and subcloned into lentiviral expression vectors with an HA tag for stable expression. For melanosome-specific pH indicators, MELOPS, purchased from addgene (#80151)[31], and GFP (Gamillus), an acid-tolerant monomeric green fluorescent protein purchased from addgene (#124837)[47] subcloned into containing IRES sequence vectors to allow for coexpression of two genes from a single transcript. For melanosome-specific calcium indicators, RCaMP, purchased from addgene (#105013) fused tyrosinase N terminal, headed for melanosomal lumen, and GFP (Gamillus) fused to MST subcloned into containing IRES sequence vectors to allow for coexpression of two genes from a single transcript. For melanosome-specific ATP sensor, iATPSnFR2 (Addgene plasmid #209652) was fused to MST at its N-terminus and subcloned into the pLKO.1 vector. HaloTag–fused iATPSnFR2 was labeled with Janelia Fluor JFX554 HaloTag Ligand (Promega, HT1030)

The following reagents were used: α-MSH (Peptide Institute, 4057-v), forskolin (TGI, F0855), melanin (sigma, M0418), bafilomycin A1 (Adipogen Life Sciences, BVT-0252-C100), biotin (nacarai, 04822-04), BAPTA-AM (nacarai, 3731-24), oligomycin (cayman,11342), 2-DG (FUJIFILM, 046-06483).

Antibodies

The following primary antibodies were used: myc (Cell Signaling Technology, 2276; 1:1000), V5 (MBL, PM003; 1:1000), FLAG (Sigma-Aldrich, F3165; 1:1000), TRP1 (Santa Cruz Biotechnology, sc-166857; 1:5000 for immunoblotting, 1:500 for immunofluorescence), ATP5a (Abcam, ab14748; 1:5000), α-tubulin (Sigma-Aldrich, T9026; 1:5000), OPA1 (BD Biosciences, 612606; 1:5000), mitofusin1 (BioLegend, 831101; dilution not applicable), mitofusin2 (Santa Cruz Biotechnology, sc-100560; dilution not applicable), tyrosinase (Santa Cruz Biotechnology, sc-20035; 1:1000), streptavidin–HRP (Vector Laboratories, SA5004; 1:1000), STIM1 (Cell Signaling Technology, 4916S; 1:1000 for immunoblotting, 1:500 for immunofluorescence), GAPDH (Santa Cruz Biotechnology, sc-32233; 1:5000), SDHA (Cell Signaling Technology, 5839S; 1:1000), and TOMM20 (Proteintech, 11802-1-AP; 1:5000). The anti-PMEL (fibril) antibody was used at a dilution of 1:2000. Anti-PMEL (fibril) was gifted from Prof. Michael S. Marks[48].

Immunoblotting

Proteins in the sample buffer were separated by SDS-PAGE and transferred to Immobilon PVDF membranes (IPVH00010, Millipore). Blots were probed with the indicated antibodies, and protein bands on the blot were visualized using Chemi-Lumi One L (07880-70, Nacalai Tesque) or Immobilon Western Chemiluminescent HRP Substrate (WBKLS0500, Millipore). Band images were captured using a LuminoGraph I imager (ATTO). Relative band intensities were quantified using Fiji/ImageJ software.

For PMEL blotting, following previous reports methods with modifications were conducted[49]. Briefly, cells were lysed in PBST buffer containing 1% Triton X-100 and protease inhibitor cocktail in PBS, served as a whole fraction, and sedimented at 125,000 g for 30 min at 4 °C. Supernatants from the initial fractionation were saved as the Triton-X-soluble fractions, and the pellets were washed once with PBST buffer before re-extraction with SDS buffer (PBST containing 1% SDS in place of Triton X-100). After sedimentation at 125,000 g for 30 min at 4 °C, the supernatants were saved as the insoluble fraction.

Immunostaining

Cells were fixed with 4% paraformaldehyde in phosphate-buffered saline (PBS) for 15 min. Fixed cells were washed three times with PBS, permeabilized with 0.1% Triton X-100 in PBS for 10 min then washed three times with PBS and blocked with 10% FBS in PBS for 10 min, all at room temperature (RT). For immunostaining, cells were incubated with the indicated primary antibodies in PBS containing 5% FBS for 2 h at RT, washed three times with PBS, and then incubated with the appropriate Alexa Fluor-conjugated secondary antibodies in PBS containing 5% FBS for 1 h. The sample was washed three times with PBS, and mounted with Fluorescent Mounting Medium (S3023, Dako), and then analyzed using a FV3000 confocal laser scanning microscope (Olympus). Slice images were acquired every 0.2 μm and reconstructed using Fiji/ImageJ software. For mitochondria and melanosome colocalization analysis, using ImageJ, the areas of extraction between mitochondria and melanosomes in a 25 x 25 μm ROI per cell were calculated.

Immunoprecipitation

After cells were cross-linked 5 mM DSP in PBS at 30 min, cells were lysed with NP-40 lysis buffer (1% Nonidet P40 Substitute, 10 mM Tris–HCl pH 7.4, 150 mM NaCl, 0.5 mM EDTA, 10 mM NaF) containing protease inhibitor cocktail (25955-11, Nacalai Tesque) and centrifuged at 15,000 g for 10 min at 4 °C. The supernatant was subjected to immunoprecipitation using the indicated antibodies and Protein G Sepharose (17–0618-01, GE Healthcare). The beads were washed four times with NP-40 lysis buffer and boiled in 2× Laemmli sample buffer (125 mM Tris–HCl pH 6.8, 10% 2-mercaptoethanol, 4% SDS, 10% sucrose, 0.01% BPB).

Lentivirus production and infection

Lenti-X 293 T Cells were seeded in 6-well plates and cultured for 2 days until they reached approximately 80% confluency at the time of transfection. Cells were transfected with lentiviral plasmid together with the packaging plasmid psPAX2 and the envelope plasmid VSV-G, using FuGENE HD Transfection Reagent (Promega). Transfections

https://doi.org/10.1038/s41467-026-70282-w

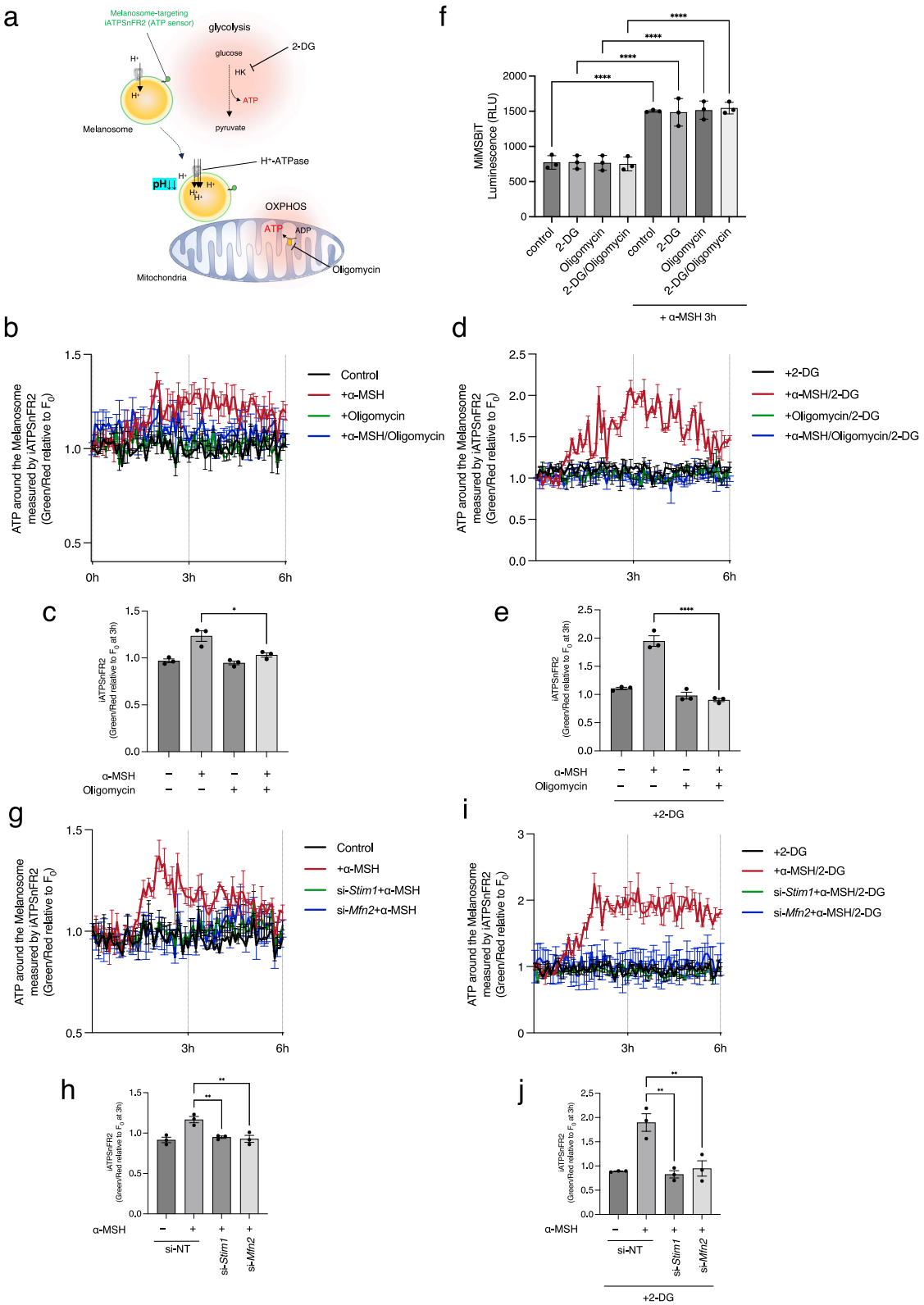

were performed in Opti-MEM, and cells were maintained in DMEM (10%FBS). On the day following transfection, half of the culture medium was replaced with fresh medium. Viral supernatants were collected 48 hours after transfection, filtered through a 0.22-μm filter, and used for infection. For lentiviral infection, target cells were incubated with viral supernatant diluted in culture medium.

Generation of MiMSBiT system stably expressing cells

Mouse melanoma B16F10 cells were kindly provided by Prof. Hideya Ando from Okayama University of Science. The pT4/HB-MiMS vector and pCAG-SB100X (Addgene #127909)[50] were transfected into B16F10 cells at a ratio of 10:1 using Lipofectamine 3000 at a ratio of 10:1 (MiMS:SB100X DNA (μg)). After 24 h, cells were selected with 2 μg/ml

Fig. 7 | Melanosome surface is exposed to mitochondrial ATP for acidification of melanosome matrix via mitochondria-melanosome contacts. a–e Changes in ATP on the surface of melanosomes due to OXPHOS under α-MSH stimulation. B16F10 cells were transfected with melanosomal outer membrane–targeted iATPSnFR2, an ATP sensor. Cells were treated with α-MSH, oligomycin, or α-MSH and oligomycin, in the absence or presence of 2-deoxy-D-glucose (2-DG). 2-DG was added 2 h prior to stimulation with α-MSH and/or oligomycin. iATPSnFR2 fluorescence (Red and Green) was monitored kinetically using a plate reader. Figure 7c and Fig. 7e show quantification of iATPSnFR2 signals at 3 h after α-MSH stimulation each. Data are presented as mean ± s.e.m. ($n = 3$). **f** OXPHOS and glycolysis do not affect mitochondria-melanosome contacts. MiMSBiT cells were treated with or without α-MSH, 2-DG, and oligomycin for 3 h before luminescence measurements. Data are mean ± s.e.m. ($n = 3$, triplicate). **g–j** Changes in ATP on the surface of melanosomes regulated by MFN2 and STIM1 under α-MSH stimulation. B16F10 cells were transfected with MFN2 or STIM1 siRNAs for 2 days, followed by transfection with melanosomal outer membrane–targeted iATPSnFR2. Cells were then stimulated with α-MSH, in the absence or presence of 2-deoxy-D-glucose (2-DG). 2-DG was added 2 h prior to α-MSH stimulation. iATPSnFR2 fluorescence was monitored kinetically using a plate reader. Figure 7h and Fig. 7j show quantification of iATPSnFR2 signals at 3 hours after α-MSH stimulation each. Data are presented as mean ± s.e.m. ($n = 3$). Statistical significance was analyzed by one-way analysis of variance (ANOVA) (**f**,**c**,**e**,**h**,**i**). P values are indicated as; $^{*}p < 0.05$; $^{**}p < 0.01$; $^{****}p < 0.0001$. n indicates independent biological experiments, unless otherwise indicated.

puromycin for 2 days, and single-cell clones were isolated in 96-well plates using a limiting dilution method.

Luciferase Assay using MiMSBiT cell

Luciferase assays using the MiMSBiT system were performed using the Nano-Glo Live Cell Assay; Nano-Glo Live Cell Substrate (N205B) and NanoBiT Buffer (Nano-Glo LCS Dilution Buffer) (N206B) (Promega, Madison, WI, USA) according to the manufacturer's instructions. For luminescence quantification, MiMSBiT cells were seeded at 0.5 or 1.0×10^4 cells per well on a 96-well white cell culture microplate (Greiner bio-one), followed by transfection of expression vectors and treatment with rotenone or antimycin A. The cell culture medium was replaced with 100 μL of buffered FluoroBrite DMEM (Gibco) or Opti-MEM, containing <1% (v/v) fetal bovine serum (FBS). 25 μL of a 1:20 mixture of Nano-Glo Live Cell Substrate (N205B) and NanoBiT Buffer was added and incubated at 37 °C for 10 min. For kinetic luminescence measurements, including the analysis shown in Fig. 3c, Nano-Glo Endurazine (N2570) (Promega, Madison, WI, USA) was used according to the manufacturer's instructions. Luminescence was then measured using a Synergy LX or HTX multimode reader (BioTek).

Kinetic fluorescent probe measurements

For kinetic fluorescent probe measurements, cells were transiently transfected or stably expressing the probe. Fluorescence signals were monitored using a Synergy HTX multimode reader (BioTek).

EM Imaging

MNT1 cells were fixed in 2.5% glutaraldehyde (Electron Microscopy Sciences, catalog no. 16022-P) in DMEM supplemented with 10% FBS at 37 °C in a 5% CO_2 incubator for 1 h. After being washed with 0.1 M phosphate buffer (0.08 M disodium hydrogen phosphate, 0.02 M sodium dihydrogen phosphate dihydrate), the cells were scraped and collected with 0.2% BSA/0.1 M phosphate buffer, followed by centrifugation at 820 g. The cells were post-fixed with 1% OsO_4 (Electron Microscopy Sciences, catalog no. 19150) and 1.5% potassium ferrocyanide (Kanto Chemical, catalog no. 32338-30) in a 0.05 M phosphate buffer for 30 min. After being rinsed three times with H_2O, the cells were stained with 1% thiocarbohydrazide (Sigma-Aldrich, catalog no. 223220) for 5 min. After being rinsed with H_2O 3 times, cells were stained with 1% OsO_4 in H_2O for 30 min. After being rinsed with H_2O 2 times at room temperature and 3 times at 50 °C, cells were treated with Walton's lead aspartate (0.635% lead nitrate (Sigma-Aldrich, catalog no. 203580), 0.4% aspartic acid (Sigma-Aldrich, catalog no. A9256), pH 5.2) at 50 °C for 20 min. After being rinsed with H_2O 3 times, the sections were followed by incubations in an ascending ethanol series (10 min each in 50% on ice and 70% on ice, 10 min each in 90%, and 5 min in 95% ethanol/ H_2O at room temperature), 5 min in 100% ethanol four times and 10 min in butyl 2,3-epoxypropyl ether (Fujifilm Wako pure chemical corporation) twice. This was followed by infiltration of Plain Resin-butyl 2,3-epoxypropyl ether for o/n at a 1:1 dilution. After incubating with 100% Plain Resin for 2 h. Finally, the resin was cured at 70 °C for 5 days. Plain Resin (Nisshin EM, catalog no. 395) was made by mixing 5.9 g of Component A, 5.9 g of Component B, and 0.21 g of Component C. Resin blocks were trimmed with a TrimTool diamond knife (Trim 45; DiATOME). 50 nm thick ultra-thin sections made with a diamond knife (Ultra 45; DiATOME) were collected on a cleaned silicon wafer strip in a Leica Ultramicrotome (UC7). These ultra-thin sections were collected on cleaned silicon wafer strips and imaged with a scanning electron microscope (JSM-IT800SHL, JEOL). Imaging was done at 1 kV accelerating voltage, 5 kV specimen voltage, 170 pA beam current, 2560 × 1920 frame size, 6 mm working distance, 12.8 × 9.6 μm field of view (pixel size 5 nm), and 5.33 μs dwell time, using the Scintillator Backscattered Electron Detector in Beam Deceleration mode.

BN-PAGE

Isolated crude mitochondria were solubilized in digitonin buffer (1% digitonin, 50 mM BisTris, 6 N HCl, 50 mM NaCl, 10% w/v Glycerol, 0.001% Ponceau S, pH 7.2) for 30 min on ice. Samples were centrifuged at 17,400 g for 30 min, and then supernatant was collected. Add 5% G-250 sample additive (Invitrogen) to the supernatant so that the final concentration is 0.5 %. Then, samples were separated on 3–12% Bis-Tris NativePAGE gels (Invitrogen), transferred to the PVDF membranes (Millipore), and immunoblotted with the indicated antibodies.

Melanin quantification assay

The B16F10 cells were collected and washed once with PBS. After the cells were detached with trypsin, they were centrifuged at 1000 x g and the supernatant was removed. The cells were then solubilized in 150 μL of 1x RIPA buffer. After that, cells were sonicated (memory 30) for 20 s using a sonicator. The lysates (100 μL) were transferred to a 96-well plate for measuring absorbance (300 nm). The remaining cell lysate was used to measure protein concentration. The blank was prepared using the B16F10 White strain, which has lost its ability to synthesize melanin. A standard curve was prepared using melanin (M0418, Sigma-Aldrich) dissolved in 1× RIPA buffer. The melanin content was normalized protein content measured by the BCA kit (Takara).

Biotin labeling and organelle membrane fraction purified by digitonin

TurboID-MFN2 expressing cells were grown in 100-mm dishes 24 h before experiments. After stimulation of α-MSH 10 μM for 3 hours, the cells were incubated with fresh medium containing D-Biotin for 30 min at 37 °C for labeling with α-MSH. The cells were washed three times with PBS. To obtain organelle membrane fraction, a digitonin fractionation assay was performed as previously described[51] with some modifications. Digitonin buffer was prepared by serial dilution of 10% digitonin (wako, 043-21371) in resuspension buffer (50 mM HEPES-KOH pH 7.4, 150 mM NaCl). The cells were pelleted by centrifugation at 500 g for 3 min at 4 °C and resuspended in PBS. After removing PBS by centrifugation, cell pellets were resuspended in 0.05% digitonin buffer, and then incubated for 10 min on ice. After centrifugation at 10,000 g for 5 min at 4 °C, the supernatant containing the cytosolic proteins was removed, and the pellet was washed with resuspension buffer. After centrifugation at 10,000 g for 5 min at 4 °C again, the supernatant was

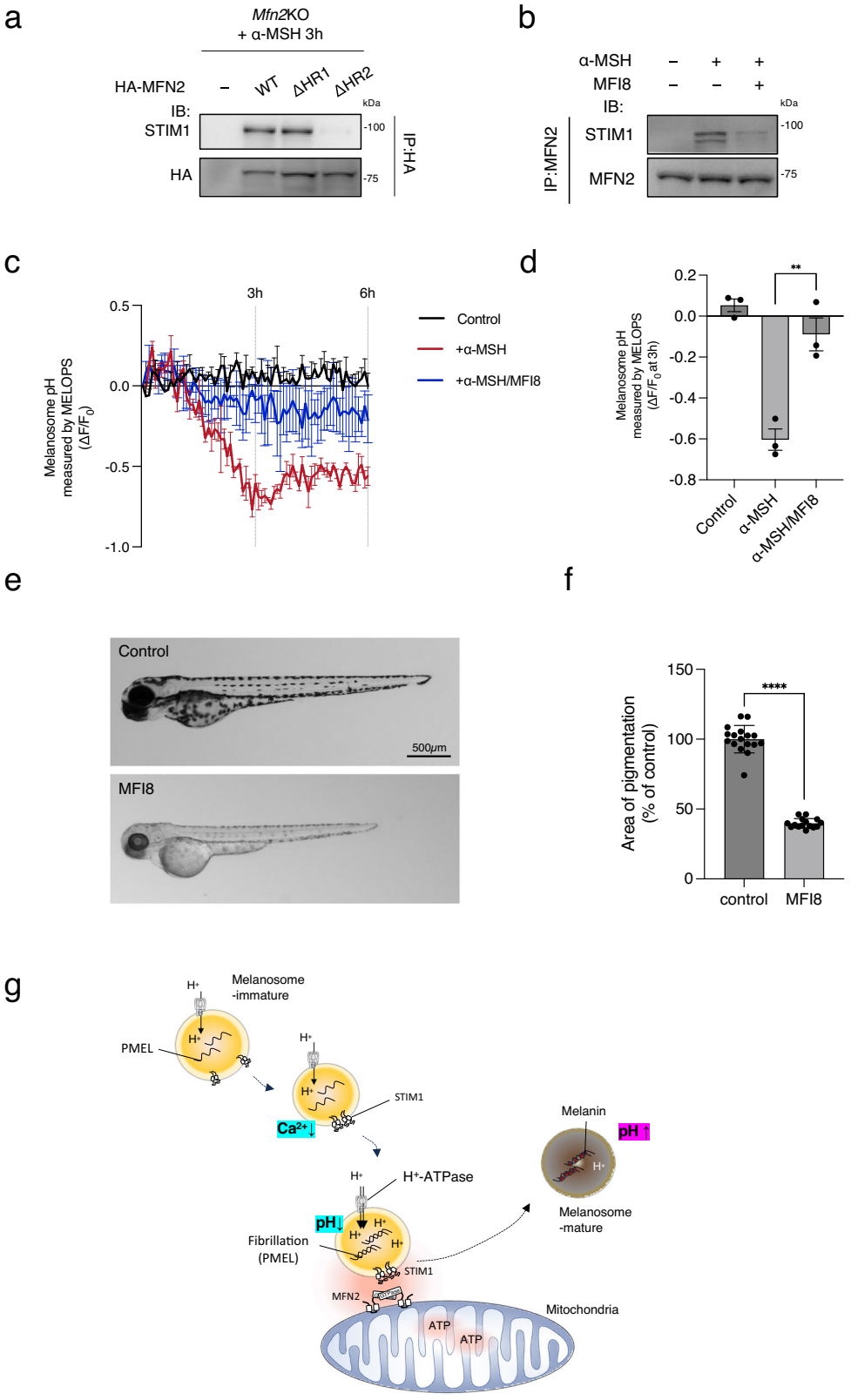

removed and the pellet was resuspended in 1% digitonin buffer. After incubation for 10 min at 4 °C, the supernatant containing membrane proteins was collected by centrifugation at 10,000 g for 5 min at 4 °C. The protein concentration of each collected supernatant was determined by BCA assay (Takara) and adjusted to 0.5 μg/μl. Each supernatant was rotated with 15 μl of Dynabeads MyOne Streptavidin C1 (streptavidin-coated magnetic beads, 65001, Invitrogen) at 4 °C overnight. The beads were washed three times with RIPA lysis buffer and pelleted on a magnetic rack. For blotting, the biotin-labeled proteins were eluted by incubating in the solution containing 0.1% SDS and 2-mM biotin for 10 min at 95 °C. The pull-down proteins on beads were subjected to LC–MS/MS analysis.

Fig. 8 | MFN2–STIM1 interaction via the HR2 domain regulates melanosome acidification and pigmentation in vivo. a STIM1 binds to the HR2 domain of MFN2. MFN2 knockout (KO) B16F10 cells were transfected with HA-tagged human MFN2 (hMFN2) wild-type or deletion mutants lacking the HR1 (Δ371–441) or HR2 (Δ693–747) domains. Transfected cells were selected uging puromycin, and cell lysates were subjected to IP followed by IB with the indicated antibodies. **b** MFI8 inhibits α-MSH–dependent STIM1–MFN2 interaction. B16F10 cells were treated with α-MSH in the presence or absence of the mitofusin inhibitor MFI8 for 3 h. Cell lysates were then subjected to IP using an antibody against endogenous MFN2, followed by IB with the indicated antibodies. **c**,**d** MFI8 suppresses α-MSH–dependent melanosomal acidification. B16F10 cells expressing melanosome matrix–targeted MELOPS were treated with α-MSH alone, or α-MSH and MFI8. MELOPS fluorescence was monitored kinetically using a plate reader. Figure 8d shows quantification of the data shown in panel c at 3 h after stimulation. Data are presented as mean ± s.e.m. ($n = 3$). **e** MFI8 suppresses pigmentation in zebrafish. Zebrafish embryos were treated with MFI8 (20 μM) several hours after fertilization. Representative images of zebrafish larvae at 3 days post-fertilization (dpf) are shown. Pigmentation was quantified by measuring the intensity of melanin in a defined region of the tail using ImageJ. Data are presented as mean ± s.e.m. (control, $n = 17$ individual zebrafish; MFI8, $n = 15$ individual zebrafish). **g** Scheme for MFN2–STIM1–mediated mitochondria–melanosome crosstalk. α-MSH–induced MFN2–STIM1 interactions promote ATP-dependent melanosome acidification, PMEL fibrillation, and melanin production. Statistical significance was analyzed by one-way analysis of variance (ANOVA) (**d**) or Student's t-test, Two-tailed (**f**). P values are indicated as; $^{**}p < 0.01$; $^{****}p < 0.0001$. n indicates independent biological experiments, unless otherwise indicated.

Sample preparation for LC-MS/MS analysis

The protein-bound beads were transferred to a new tube, and washed with 50 mM ammonium bicarbonate buffer twice. The beads were suspended in 100 μL of 50 mM ammonium bicarbonate buffer containing 10 mM dithiothreitol (DTT) and incubated at 5 °C for 15 min. After discarding the supernatant, 100 μL of 100 mM iodoacetamide (IAA) in 50 mM ammonium bicarbonate buffer was added to the beads, and the suspension was further incubated at room temperature for 30 min in the dark. After discarding the supernatant, the proteins on beads were digested by 0.5 μg of Trypsin/Lys-C mix (mass spec grade, Promega) in 100 μL of 50 mM ammonium bicarbonate buffer at 37 °C overnight with shaking. The supernatant was collected in a new tube and acidified with 10% trifluoroacetic acid to quench the reaction, then desalted by StageTip embedded Empore™ SDB-XC disks (GL Science) according to the previously published literature[52]. The desalted eluate was dried *in vacuo* and dissolved in 2% MeCN, 0.1% formic acid in distilled water for LC-MS/MS measurement. Biotin-treated and biotin-untreated samples were prepared in triplicates, respectively.

LC-MS/MS analysis and data processing

LC-MS/MS analysis was performed on an Ultimate 3000 RSLCnano system (Thermo Fisher Scientific) coupled to a Q Exactive hybrid quadrupole-Orbitrap mass spectrometer (Thermo Fisher Scientific) equipped with a nano electrospray ionization source. The nanoLC system was equipped with a trap column (C18 PepMap 100, 0.3 × 5 mm, 5 μm, Thermo Fisher Scientific) and an analytical column (NTCC-360/75-3-125, Nikkyo Technos, Tokyo, Japan). Peptide separation was performed using 60 min gradient of water containing 0.1% formic acid (mobile phase A) and acetonitrile containing 0.1% formic acid (mobile phase B) at a flow rate of 300 nL/min. The elution was set as follows: 0–3 min, 2% B; 3–63 min, 2%–40% B; 63–65 min, 40%–95% B; 65–75 min, 95% B; 75–77 min, 95%–2% B; 77–90 min, 2% B. Measurements were performed in duplicate. The mass spectrometer was operated in data-dependent acquisition (DDA) mode. MS parameters were set as follows: spray voltage, 2.0 kV; capillary temperature, 275 °C; S-lens RF level, 50; scan type, full MS; scan range, m/z 350–1500; resolution, 70,000; polarity, positive; automatic gain control target, 3×10^6; maximum injection time, 100 msec. MS/MS parameters were set as follows: resolution, 17,500; automatic gain control target, 1×10^5; maximum injection time, 60 msec; normalized collision energy, 27; dynamic exclusion, 15 s; loop count, 10; isolation window, 1.6 m/z; charge exclusion, unassigned, 1, 8, >8. The identification of peptides and proteins, and label-free quantification (LFQ) of the detected peptides were performed by using Proteome Discoverer (version 3.0, Thermo Fisher Scientific). The analytical parameters used for the data processing of peptides were as follows: parent mass error tolerance, 10.0 ppm; fragment mass error tolerance, 0.02 Da; search engine, sequest HT; protein database, SwissProt (Mus musculus); enzyme name, trypsin/P (full); maximum number of missed cleavages, 2; FDR confidence <0.01; dynamic modification, oxidation (methionine), phosphorylation (serine, threonine, tyrosine), acetyl (lysine), Met-loss (methionine), and Metloss+ acetyl (methionine); static modification, carbamidomethyl (cysteine). Label-free quantification parameters for the detected peptides were set as follows: precursor quantification, precursor abundance based on area; normalization mode, none; and hypothesis test, t-test (background based). Abundance ratio and *p*-values were calculated by Proteome Discoverer. From the biotinylated proteins, we selected the top 25 proteins with the highest ratio that met the criteria of $p \leq 0.05$ and and high FDR confidence. Proteins with no quantitative values in the biotin-untreated sample group were excluded from the results. The mass spectrometry data were deposited to the ProteomeXchange Consortium via the jPOST partner repository with the dataset identifier (JPST003803; PXD063939). Among them, candidate genes that were not localized to mitochondria or the cytoplasm were further examined using siRNA screening. A volcano plot of biotinylated proteins proximally labeled by TurboID was generated using VolcanoR[53].

Zebrafish maintenance and live imaging

Zebrafish were maintained in a MEITO system (MEITOSUIEN Co. Ltd., Aichi, Japan) at 28 °C under a 14/10 h light/dark cycle. Zebrafish embryos were obtained by natural mating. Zebrafish larvae were maintained in E3 medium (5 mM NaCl, 0.17 mM KCl, 0.33 mM CaCl2, 0.33 mM MgSO4) in the presence of MF18 (20 μM) or DMSO at 28 °C under a 14/10 h light/dark cycle. Live Imaging analyses were performed by Axio Zoom. V 16 stereomicroscope (Carl Zeiss, Oberkochen, Germany). The present analysis is approved by Kanazawa University Animal Experiment Committee.

Statistics & Reproducibility

Data are presented as mean ± s.e.m. and expressed as percentages or multiples relative to the values in control cells. Statistical significance was analyzed using Prism 9 software (GraphPad Software). Statistical significance was analyzed by either one-way analysis of variance followed by Bonferroni's test, as appropriate. P values are indicated as $^{*}p < 0.05$; $^{**}p < 0.01$; $^{***}p < 0.001$; $^{****}p < 0.0001$; n.s., not significant. No statistical method was used to predetermine sample size. No data were excluded from the analyses. The experiments were not randomized. The investigators were not blinded to allocation during experiments and outcome assessment. All experiments were independently repeated at least three times with similar results unless otherwise stated. In experiments, representative images (including immunoblotting and immunofluorescence) are shown from experiments that were independently repeated at least three times with similar results, unless otherwise stated. For electron microscopy analyses, experiments were performed once due to technical constraints. Multiple cells and organelles were independently analyzed from the same experiment, and quantitative analyses were based on these independent cellular observations.

Data availability

The mass spectrometry proteomics data generated in this study have been deposited in the ProteomeXchange Consortium via the jPOST

partner repository under the dataset identifiers JPST003803 and PXD063939. Source data underlying all figures are provided with this paper. Other data supporting the findings of this study are available from the corresponding authors. Source data are provided with this paper.

References

1. Voeltz, G. K., Sawyer, E. M., Hajnóczky, G. & Prinz, W. A. Making the connection: how membrane contact sites have changed our view of organelle biology. *Cell* **187**, 257–270 (2024).
2. Scorrano, L. et al. Coming together to define membrane contact sites. *Nat. Commun.* **10**, 1287 (2019).
3. Tábara, L. C., Segawa, M. & Prudent, J. Molecular mechanisms of mitochondrial dynamics. *Nat. Rev. Mol. Cell Biol.* **26**, 123–146 (2025).
4. Jenkins, B. C. et al. Mitochondria in disease: changes in shapes and dynamics. *Trends Biochem. Sci.* **49**, 346–360 (2024).
5. Copeland, D. E. & Dalton, A. J. An association between mitochondria and the endoplasmic reticulum in cells of the pseudobranch gland of a teleost. *J. Biophys. Biochem. Cytol.* **5**, 393–396 (1959).
6. de Brito, O. M. & Scorrano, L. Mitofusin 2 tethers endoplasmic reticulum to mitochondria. *Nature* **456**, 605–610 (2008).
7. Rizzuto, R. et al. Ca(2+) transfer from the ER to mitochondria: when, how and why. *Biochim. Biophys. Acta* **1787**, 1342–1351 (2009).
8. Giacomello, M. & Pellegrini, L. The coming of age of the mitochondria-ER contact: a matter of thickness. *Cell Death Differ.* **23**, 1417–1427 (2016).
9. Rowland, A. A. & Voeltz, G. K. Endoplasmic reticulum-mitochondria contacts: function of the junction. *Nat. Rev. Mol. Cell Biol.* **13**, 607–625 (2012).
10. Daniele, T. et al. Mitochondria and melanosomes establish physical contacts modulated by Mfn2 and involved in organelle biogenesis. *Curr. Biol.* **24**, 393–403 (2014).
11. Raiborg, C., Malerød, L., Pedersen, N. M. & Stenmark, H. Differential functions of Hrs and ESCRT proteins in endocytic membrane trafficking. *Exp. Cell Res.* **314**, 801–813 (2008).
12. Raiborg, C., Wesche, J., Malerød, L. & Stenmark, H. Flat clathrin coats on endosomes mediate degradative protein sorting by scaffolding Hrs in dynamic microdomains. *J. Cell Sci.* **119**, 2414–2424 (2006).
13. Raposo, G. & Marks, M. S. Melanosomes-dark organelles enlighten endosomal membrane transport. *Nat. Rev. Mol. Cell Biol.* **8**, 786–797 (2007).
14. Raiborg, C. & Stenmark, H. The ESCRT machinery in endosomal sorting of ubiquitylated membrane proteins. *Nature* **458**, 445–452 (2009).
15. Wiriyasermkul, P., Moriyama, S. & Nagamori, S. Membrane transport proteins in melanosomes: regulation of ions for pigmentation. *Biochim. Biophys. Acta Biomembr.* **1862**, 183318 (2020).
16. Le, L., Sirés-Campos, J., Raposo, G., Delevoye, C. & Marks, M. S. Melanosome biogenesis in the pigmentation of mammalian skin. *Integr. Comp. Biol.* **61**, 1517–1545 (2021).
17. Cui, R. et al. Central role of p53 in the suntan response and pathologic hyperpigmentation. *Cell* **128**, 853–864 (2007).
18. Buscà, R. & Ballotti, R. Cyclic AMP a key messenger in the regulation of skin pigmentation. *Pigment Cell Res.* **13**, 60–69 (2000).
19. Cheli, Y. et al. {alpha}MSH and Cyclic AMP elevating agents control melanosome pH through a protein kinase A-independent mechanism. *J. Biol. Chem.* **284**, 18699–18706 (2009).
20. Hirobe, T. Stimulation of dendritogenesis in the epidermal melanocytes of newborn mice by melanocyte-stimulating hormone. *J. Cell Sci.* **33**, 371–383 (1978).
21. Zhou, D. et al. Mammalian pigmentation is regulated by a distinct cAMP-dependent mechanism that controls melanosome pH. *Sci. Signal.* **11**, eaau7987 (2018).
22. Hearing, V. J. Biochemical control of melanogenesis and melanosomal organization. *J. Investig. Dermatol. Symp. Proc.* **4**, 24–28 (1999).
23. Bhatnagar, V., Anjaiah, S., Puri, N., Darshanam, B. N. & Ramaiah, A. pH of melanosomes of B 16 murine melanoma is acidic: its physiological importance in the regulation of melanin biosynthesis. *Arch. Biochem. Biophys.* **307**, 183–192 (1993).
24. Pfefferkorn, C. M., McGlinchey, R. P. & Lee, J. C. Effects of pH on aggregation kinetics of the repeat domain of a functional amyloid, Pmel17. *Proc. Natl. Acad. Sci. USA* **107**, 21447–21452 (2010).
25. Watt, B., van Niel, G., Raposo, G. & Marks, M. S. PMEL: a pigment cell-specific model for functional amyloid formation. *Pigment Cell Melanoma Res* **26**, 300–315 (2013).
26. McGlinchey, R. P. et al. The repeat domain of the melanosome fibril protein Pmel17 forms the amyloid core promoting melanin synthesis. *Proc. Natl. Acad. Sci. USA* **106**, 13731–13736 (2009).
27. Shiiba, I. et al. ER-mitochondria contacts mediate lipid radical transfer via RMDN3/PTPIP51 phosphorylation to reduce mitochondrial oxidative stress. *Nat. Commun.* **16**, 1508 (2025).
28. Ishida, M., Arai, S. P., Ohbayashi, N. & Fukuda, M. The GTPase-deficient Rab27A(Q78L) mutant inhibits melanosome transport in melanocytes through trapping of Rab27A effector protein Slac2-a/melanophilin in their cytosol: development of a novel melanosome-targetinG tag. *J. Biol. Chem.* **289**, 11059–11067 (2014).
29. Tilokani, L., Nagashima, S., Paupe, V. & Prudent, J. Mitochondrial dynamics: overview of molecular mechanisms. *Essays Biochem* **62**, 341–360 (2018).
30. Naon, D. et al. Splice variants of mitofusin 2 shape the endoplasmic reticulum and tether it to mitochondria. *Science* **380**, eadh9351 (2023).
31. Ambrosio, A. L., Boyle, J. A., Aradi, A. E., Christian, K. A. & Di Pietro, S. M. TPC2 controls pigmentation by regulating melanosome pH and size. *Proc. Natl. Acad. Sci. USA* **113**, 5622–5827 (2016).
32. Branon, T. C. et al. Efficient proximity labeling in living cells and organisms with TurboID. *Nat. Biotechnol.* **36**, 880–887 (2018).
33. Dooley, C. M. et al. Slc45a2 and V-ATPase are regulators of melanosomal pH homeostasis in zebrafish, providing a mechanism for human pigment evolution and disease. *Pigment Cell Melanoma Res.* **26**, 205–217 (2013).
34. Marvin, J. S. et al. iATPSnFR2: a high-dynamic-range fluorescent sensor for monitoring intracellular ATP. *Proc. Natl. Acad. Sci. Usa.* **121**, e2314604121 (2024).
35. Zacharioudakis, E. et al. Modulating mitofusins to control mitochondrial function and signaling. *Nat. Commun.* **13**, 3775 (2022).
36. Sheets, L., Ransom, D. G., Mellgren, E. M., Johnson, S. L. & Schnapp, B. J. Zebrafish melanophilin facilitates melanosome dispersion by regulating dynein. *Curr. Biol.* **17**, 1721–1734 (2007).
37. Luik, R. M., Wang, B., Prakriya, M., Wu, M. M. & Lewis, R. S. Oligomerization of STIM1 couples ER calcium depletion to CRAC channel activation. *Nature* **454**, 538–542 (2008).
38. Zhang, Z., Gong, J., Sviderskaya, E. V., Wei, A. & Li, W. Mitochondrial NCKX5 regulates melanosomal biogenesis and pigment production. *J. Cell Sci.* **132**, jcs232009 (2019).
39. Le, L. et al. SLC45A2 protein stability and regulation of melanosome pH determine melanocyte pigmentation. *Mol. Biol. Cell* **31**, 2687–2702 (2020).
40. Hellström, A. R. et al. Inactivation of Pmel alters melanosome shape but has only a subtle effect on visible pigmentation. *PLoS Genet.* **7**, e1002285 (2011).
41. Rochin, L. et al. BACE2 processes PMEL to form the melanosome amyloid matrix in pigment cells. *Proc. Natl. Acad. Sci. USA* **110**, 10658–10663 (2013).
42. Motiani, R. K. et al. STIM1 activation of adenylyl cyclase 6 connects Ca(2+) and cAMP signaling during melanogenesis. *EMBO J.* **37**, e97597 (2018).

43. Sugiura, A. et al. MITOL regulates endoplasmic reticulum-mitochondria contacts via mitofusin2. *Mol. Cell* **51**, 20–34 (2013).
44. Ban-Ishihara, R., Ishihara, T., Sasaki, N., Mihara, K. & Ishihara, N. Dynamics of nucleoid structure regulated by mitochondrial fission contributes to cristae reformation and release of cytochrome c. *Proc. Natl. Acad. Sci. USA* **110**, 11863–11868 (2013).
45. Wang, Y. et al. Regulated complex assembly safeguards the fidelity of Sleeping Beauty transposition. *Nucleic Acids Res.* **45**, 311–326 (2017).
46. Akagi, T., Sasai, K. & Hanafusa, H. Refractory nature of normal human diploid fibroblasts with respect to oncogene-mediated transformation. *Proc. Natl. Acad. Sci. USA* **100**, 13567–13572 (2003).
47. Shinoda, H. et al. Acid-tolerant monomeric GFP from olindias formosa. *Cell Chem. Biol.* **25**, 330–338 (2018).
48. Leonhardt, R. M., Vigneron, N., Rahner, C., Van den Eynde, B. J. & Cresswell, P. Endoplasmic reticulum export, subcellular distribution, and fibril formation by Pmel17 require an intact N-terminal domain junction. *J. Biol. Chem.* **285**, 16166–16183 (2010).
49. Beyers, W. C., Detry, A. M. & Di Pietro, S. M. OCA7 is a melanosome membrane protein that defines pigmentation by regulating early stages of melanosome biogenesis. *J. Biol. Chem.* **298**, 102669 (2022).
50. Strom, A. R. et al. HP1α is a chromatin crosslinker that controls nuclear and mitotic chromosome mechanics. *eLife* **10**, e63972 (2021).
51. Ito, N. et al. MITOL regulates phosphatidic acid-binding activity of RMDN3/PTPIP51. *J. Biochem.* **171**, 529–541 (2022).
52. Rappsilber, J., Mann, M. & Ishihama, Y. Protocol for micro-purification, enrichment, pre-fractionation and storage of peptides for proteomics using StageTips. *Nat. Protoc.* **2**, 1896–1906 (2007).
53. Goedhart, J. & Luijsterburg, M. S. VolcaNoseR is a web app for creating, exploring, labeling and sharing volcano plots. *Sci. Rep.* **10**, 20560 (2020).

Acknowledgements

We thank Michael S. Marks for the generous gift of PMEL fibril (I51) antibody. We thank Saki Asada for technical assistance. This study was partially supported by the MEXT/JSPS KAKENHI [Grant Nos. 22K15399, 22H05574, 24H01327, and 24K18382 (for IS), 23K14185 and 22K20637 (for NI), 21K06844 (for RI), 23K02691, 20H04911 and 20H03454 (for SY)], the Uehara Memorial Foundation (for IS and SY), the Kowa Life Science Foundation (to IS)], the Takeda Science Foundation (2025) (for SY), the Daiichi Sankyo Foundation of Life Science (for SY) and AMED [Grant No. JP20gm5010002 and JP25gm2110001 (to SY)].

Author contributions

I.S. and S.Y. designed the experiments; I.S., N.I., K.U., Y.A., H.O., Y.I., and F.Y. performed the experiments; I.S. and S.Y. analyzed and interpreted the data; Y.M., H.A., S.N., Y.A., K.N., Y.H., and R.I. assisted in the analysis; I.S. and S.Y. wrote the paper.

Competing interests

The authors declare no competing interests.

Additional information

Supplementary information The online version contains supplementary material available at https://doi.org/10.1038/s41467-026-70282-w.

Correspondence and requests for materials should be addressed to Isshin Shiiba or Shigeru Yanagi.

Peer review information *Nature Communications* thanks Qing Deng, David Peeney and the other, anonymous, reviewers for their contribution to the peer review of this work. A peer review file is available.